



Late Cenozoic tectonic activity of the Altyn Tagh range: Constraints from sedimentary records from the Western Qaidam Basin, NE Tibetan Plateau

Tao Zhang^{a,*}, Xiaomin Fang^{a,b}, Yadong Wang^c, Chunhui Song^d, Weilin Zhang^a, Maodu Yan^a, Wenxia Han^e, Dawen Zhang^a

^a Institute of Tibetan Plateau Research, Chinese Academy of Sciences & CAS Center for Excellence in Tibetan Plateau Earth Sciences, Beijing 100101, China

^b University of Chinese Academy of Sciences, Beijing 100049, China

^c Gansu Provincial Key Laboratory of Petroleum Resources, Key Laboratory of Petroleum Resources Research, Institute of Geology and Geophysics, Chinese Academy of Sciences, Lanzhou 730000, China

^d School of Earth Sciences & Key Laboratory of Western China's Mineral Resources of Gansu Province, Lanzhou University, Lanzhou 730000, China

^e Key Laboratory of Salt Lake Geology and Environment of Qinghai Province, Qinghai Institute of Salt Lakes, Chinese Academy of Sciences, Xining 810008, China

ARTICLE INFO

Keywords:

Sedimentary records
Tectonic activity
Late Cenozoic
Altyn Tagh range
Qaidam Basin

ABSTRACT

The Altyn Tagh range (ATR) is the northern geological boundary of the Tibetan Plateau and plays a key role in accommodating its Cenozoic lithospheric deformation. However, knowledge of the structural style and age of uplift of the ATR is limited and controversial. The Qaidam Basin, in the southeast side of the ATR, provides an outstanding field laboratory for understanding the history and mechanisms of ATR growth. This study presents a detailed sedimentological analysis of a 1040-m-thick late Cenozoic (~17–5.0 Ma) sedimentary sequence from the western Qaidam Basin, together with the analysis of sedimentological data from nearby boreholes and sections. Our aims were to determine the spatiotemporal evolution of the sedimentary sequences in the study area and to explore their response to late Cenozoic tectonic activity in the ATR. The results show three major intervals of the sedimentary characteristics in the study area: ~ > 17–16 Ma, 10 Ma and < 5 Ma, which are closely related to the development of unconformities and growth strata recorded by high-resolution seismic reflection profiles. Combining the results with a comprehensive provenance analysis and with published records of regional climate change and tectonic activity, we discuss the possible factors responsible for the variations in the sedimentary characteristics of the studied sections. We conclude that significant tectonic responses in the western Qaidam Basin during the late Cenozoic were caused by three stages of tectonic activity of the ATR, at ~ > 17–16 Ma, ~16–10 Ma and ~10 Ma, during which the ATR respectively experienced tectonic uplift, fast strike-slip motion and intense uplift.

1. Introduction

The collision of the Indian and Asian plates in the Cenozoic had major global effects, including changes in seawater geochemistry, inception of the Indian monsoon, development of the Tibetan Plateau, and widely distributed deformation and extrusion of continental blocks (Argand, 1924; Raymo and Ruddiman, 1988; Ruddiman and Kutzbach, 1989; Molnar and England, 1990; An et al., 2001). India has penetrated northwards into Tibet and the surrounding region by > 2000 km over the past ~55 Ma (Molnar and Tapponnier, 1975). However, there is considerable debate regarding the mechanisms of strain accommodation within the Tibetan Plateau associated with the India-Asia convergence. The mechanisms can be represented as two basic models: (1) homogeneous crustal thickening and surface uplift of the Tibetan

Plateau (England and Houseman, 1986; Molnar et al., 1993; Searle, 1996), and (2) eastward/outward extrusion of the entire Tibetan Plateau and southeastern Asia, especially away from the indenting Indian plate (e.g., Molnar and Tapponnier, 1975; Armijo et al., 1989; Avouac and Tapponnier, 1993; Métivier et al., 1998; Tapponnier et al., 2001; Wang et al., 2008, 2014; Cheng et al., 2015a; Fang et al., 2013; Xu et al., 2017). To accommodate extrusion of the Tibetan crust, large-scale displacement along the principal strike-slip fault zones is needed by the second model (e.g., Searle, 1996; Tapponnier et al., 2001). The Altyn Tagh Range (ATR), including the Altyn Tagh Mountains (ATM) and the left-lateral strike-slip Altyn Tagh fault (ATF), serves as the northern geological boundary of the Tibetan Plateau (Fig. 1a, b). It plays an important role in accommodating crustal deformation and thus is an ideal place for exploring the dynamics of plateau formation

* Corresponding author.

E-mail address: zhangtao@itpcas.ac.cn (T. Zhang).

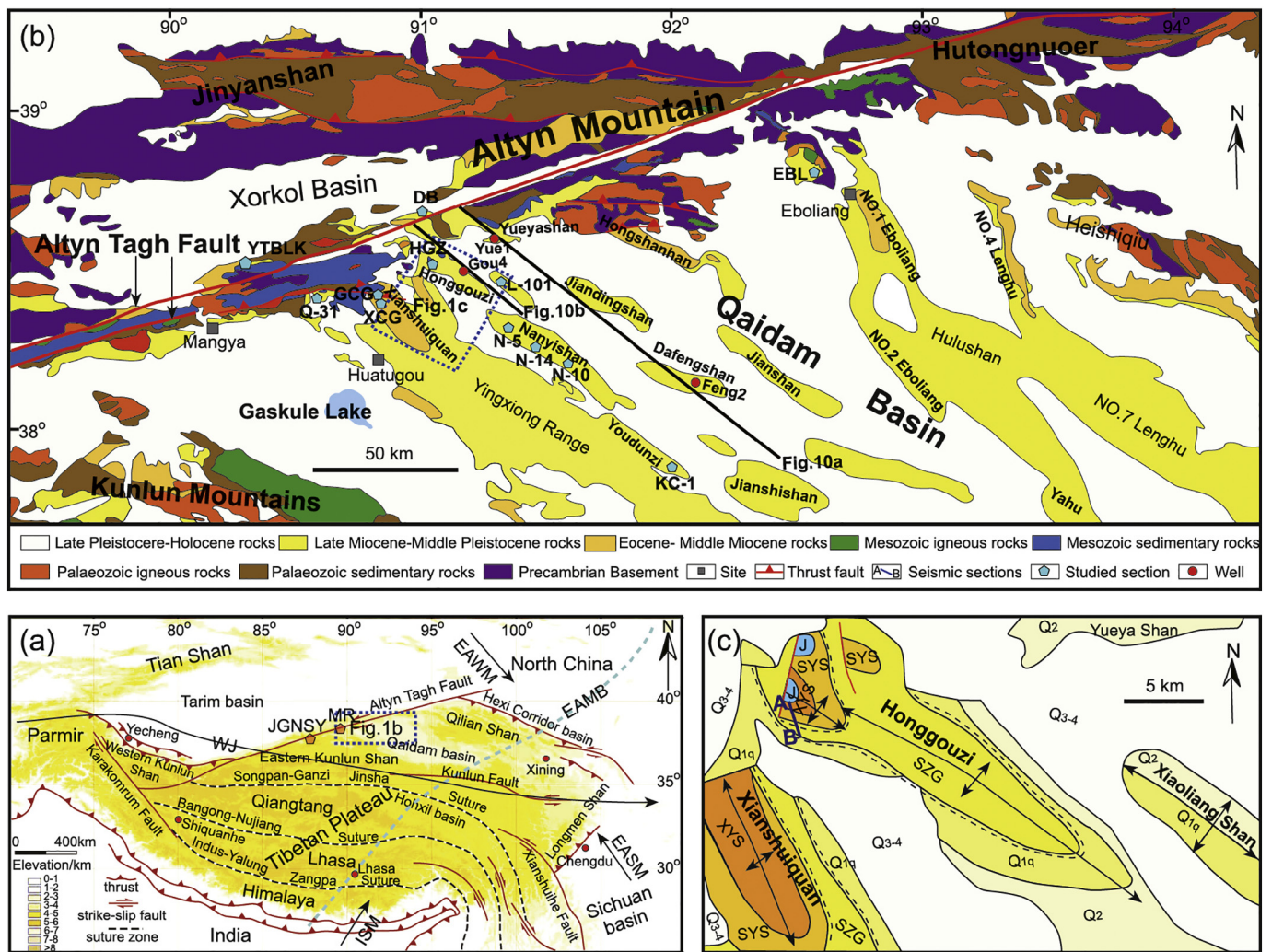


Fig. 1. (a) Topography and major tectonic units of the Tibetan plateau, and the major atmospheric circulation systems influencing Asia. EAMW: East Asian monsoon Boundary; ISM: Indian summer monsoon; EASM: East Asian summer monsoon; EAWM: East Asian winter monsoon; WJ: Westerly jet; JGNSY: Jiangnanashayi section; MR: Miran river section. (b) Simplified geological map of the western Qaidam Basin and the central segment of the Altyn Tagh range (modified from Wu et al., 2012). XCG: Xichagou section; GCG: Ganchaigou section; HGZ: Honggouzi section; EBL: Eboliang section; YTLK: Yitunbulake section; DB: Daban section; Q-31: Qi-31 well; L-101: Liang-101 well; N-5: Nan-5 well; N-10: Nan-10 well; N-14: Nan-14 well; KC-1: Kaican-1 well. (c) Detailed geologic map of the Honggouzi anticline, adapted from the Geological Map of the Qaidam Basin, and showing the location of the Honggouzi section (A–B).

(Molnar and Tapponnier, 1975; Wittlinger et al., 1998; Yue and Liou, 1999; Jolivet et al., 2001; Yin et al., 2002; Yue et al., 2004a, 2004b; Searle et al., 2011; Cheng et al., 2015b, 2016a). The region is also significantly influenced by the Asian monsoon and the westerly jet, and therefore changes in its morphology will exert a profound influence on the regional climate as well as on the evolution of the Asian monsoon and westerly jet systems (Wang et al., 1999; Miao et al., 2011, 2016a, 2016b; Zhang et al., 2012a; Jian et al., 2014; Song et al., 2014; Liu et al., 2015) (Fig. 1a). Furthermore, as an area with active inter-continental mountain belts, the history of mountain building of the ATR can potentially be interpreted from the record of sediment accumulation in the adjacent Qaidam, Tarim and Xorkol Basins (Yue and Liou, 1999; Sobel et al., 2001; Tapponnier et al., 2001; Yin et al., 2002; Cowgill et al., 2003; Yue et al., 2004a, 2004b; Ritts et al., 2004, 2008; Wang et al., 2006; Zhuang et al., 2011a; Chang et al., 2012, 2015; Wu et al., 2012; Lu et al., 2014; Pan et al., 2015; Zhang et al., 2016a). Therefore, precise dating of the Cenozoic tectonic deformation in the ATR is essential for understanding the possible mechanisms of Tibetan Plateau uplift and its effects on basin-mountain coupling and climatic change. In the past few decades, studies on the foregoing topics were focused primarily on the constitution and configuration of the Altyn

Tagh tectonic zone, tectonic activity in the Mesozoic-early Cenozoic, the characteristics of the motion of the strike-slip fault and strike-slip displacement, and the evaluation of the strike-slip rate (e.g., Tapponnier et al., 1986; CSBS, 1992; Wang, 1997; Jolivet et al., 1999, 2001; Sobel et al., 2001; Yue et al., 2001, 2004a, 2004b, 2005; Cowgill et al., 2003; Ritts et al., 2004; Darby et al., 2005; Wang et al., 2005, 2015; Li et al., 2006; Liu et al., 2007; Searle et al., 2011; Cheng et al., 2015b, 2016a). However, the detailed tectonic activity history of the ATR from the Miocene to the Pliocene is still disputed and different deformations times have been suggested: e.g., inception of the ATF at late Oligocene-earliest Miocene (Yue et al., 2001) or at 15 Ma (Wu et al., 2012); fast strike-slip motion for ATF between 22 and 15 Ma (Lu et al., 2014, 2016) or at 15 Ma (Chang et al., 2015); enhanced tectonic activity within the ATR since Miocene time (Cheng et al., 2016a) or at ca. 12 Ma (Lu and Lu and Xiong, 2009); accelerated uplift of the ATR at ca. 10 Ma (Jolivet et al., 2001; Zhang et al., 2016a) or at ca. 8 Ma (Wan et al., 2001; Chen et al., 2006; Pan et al., 2015; Zhang et al., 2016b); and intensive activity of the ATR at 3.2 Ma (Chang et al., 2012) or at 2.6 Ma (Li et al., 2006; Pan et al., 2015) and so on.

The Qaidam Basin, located in the southeast side of the ATR (Fig. 1a, b), has had an inland drainage system since the Eocene (Yin et al.,

2008a; Bush et al., 2016; Cheng et al., 2016b). Cenozoic sediments derived from the surrounding mountains, with a maximum thickness of ~13,400 m, have filled the basin (GMRBQP, 1991; Huang et al., 1996; Wang et al., 2006; Fang et al., 2007). Consequently, the Qaidam Basin is considered as the ideal place to record the processes of basin infilling, mountain uplift, and the spatiotemporal patterns of weathering and range exhumation. The Honggouzi (HGZ) section, in the western Qaidam Basin, is a middle Miocene-to-Pliocene sequence of fluvial-lacustrine sediments with a robust chronology (~17–5 Ma) (Fang et al., 2006; Song et al., 2014; Zhang et al., 2016a) (Fig. 1c). The section provides an excellent opportunity to explore the relationship between tectonic activity and climatic changes in the region. In this study, we conducted detailed sedimentological analyses of the HGZ section, together with an analysis of nearby drilling cores and other outcrop sections. The aim was to characterize the spatiotemporal evolution of the sedimentary characteristics of the western Qaidam Basin from the Mid-Miocene to the earliest Pliocene. Subsequently, we combined the results with tectonic investigations and seismostratigraphic analysis to characterize the way in which the sedimentary characteristics of the western Qaidam Basin responded to the tectonic activity history of the ATR during the late Cenozoic.

2. Geological setting, stratigraphy and age constraints

Located along the northern boundary of the Tibetan Plateau, the ATR separates the Qaidam Basin to the southeast and the Tarim Basin to the northwest (Fig. 1a, b). The bedrock of the ATR is mainly composed of Paleozoic igneous and sedimentary rocks and Precambrian metamorphic and igneous rocks (e.g. GMRBQP, 1991; Yin et al., 2002; Cheng et al., 2016a, 2016b). The ATR may have experienced tectonic exhumation and polystage crustal deformation from the Jurassic to the Holocene (e.g., Tapponnier et al., 1986; CSBS, 1992; Jolivet et al., 1999, 2001; Delville et al., 2001; Yue et al., 2001; Yin et al., 2002; Li et al., 2006; Liu et al., 2007; Zhang et al., 2012b; Cheng et al., 2015a, 2015b, 2016a, 2016b). In the southwestern and northeastern ATR, the western Kunlun and Qilian Shan thrust belts are linked to the > 1600-km-long ENE-trending ATF, respectively (Fig. 1a) (GMRBQP, 1991; CSBS, 1992).

The rhombus-shaped Qaidam Basin is the largest petroliferous sedimentary basin of the Tibetan Plateau (Fig. 1a, b) which is surrounded by the Eastern Kunlun Mountains to the south, the Qilian Mountains to the northeast, and the ATR to the northwest. The nature of the Qaidam basement is relatively poorly defined due to its being covered by up to ~16 km of Mesozoic-Cenozoic sedimentary rocks (Cheng et al., 2017); however, the results of geological investigations and hydrocarbon exploration have revealed an unconformity between the basement and the overlying Mesozoic and Cenozoic strata (Xia et al., 2001; Yin et al., 2002, 2008a, 2008b; Meng and Fang, 2008). The Mesozoic strata are mainly distributed in the northeastern and northern parts of the basin (GMRBQP, 1991). Thick and continuous Cenozoic sediments are deposited over the entire basin. Previous studies have established a lithostratigraphic framework for the Qaidam Basin. The Cenozoic stratigraphy includes seven formations (Fms.) across almost the entire basin: Qigequan (QGQ), Shizigou (SZG), Shang Youshashan (SYSS), Xia Youshashan (XYSS), Shang Ganchaigou (SGCG), Xia Ganchaigou (XGCG) and Lulehe (LLH). The respective boundaries of the formations are designated T₀, T₁, T₂, T₃, T₄, T₅ and T_R. Lithostratigraphic correlation and comparisons among the different horizons throughout the entire basin can be accomplished using data from seismic profiles and oil exploration wells (e.g., Zhang et al., 2016a, and references therein).

The present study focuses on the well-exposed HGZ section (91°3′ E, 38° 34′ N, 1040-m-thick). The outcrop is located on the southwestern limb of the Honggouzi Fold of the western Qaidam Basin (Fig. 1b, c). The HGZ section contains the following formations: XYSS (0–120 m), SYSS (120–596 m), SZG. (596–1014 m), and QGQ (1014–1040 m)

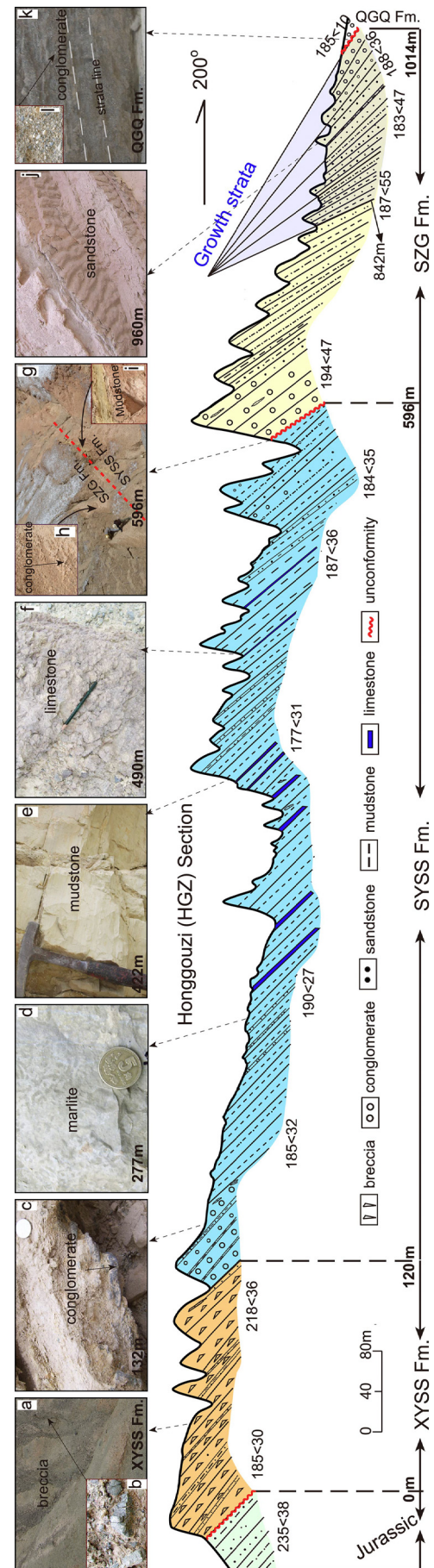


Fig. 2. Photographs and diagrams showing the studied HGZ section in the Honggouzi anticline. The extended grey triangle indicates the occurrence of growth strata.

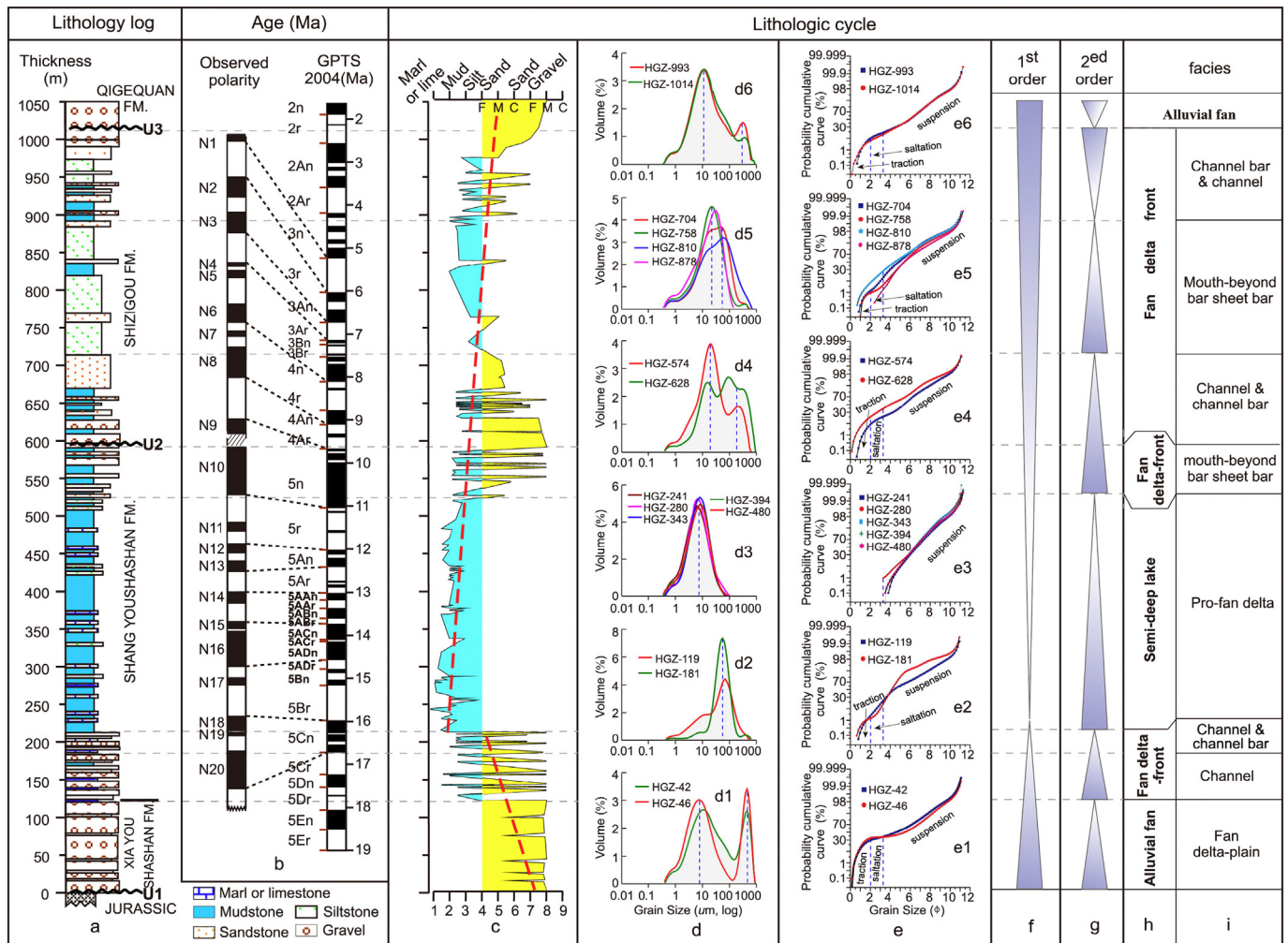


Fig. 3. (a) Lithology, (b) paleomagnetic results (after Fang et al., 2006 and Song et al., 2014), (c) semi-quantitative representation of the lithology, (d) grain-size frequency distribution curves and (e) grain-size cumulative frequency curves of representative bulk samples, (f, g) sedimentary cycles (h, i) facies (h, i), of the HGZ section.

(Fig. 2). The XYSS Fm. lies unconformably (U1) on Jurassic strata (Figs. 1c and 2) and the SYSS Fm. lies below the SZG Fm. in a small angular unconformity (U2), while the SZG Fm. lies beneath the QGQ Fm. in a large angular unconformity (U3) (Fig. 2). Interestingly, the XYSS, SYSS, and SZG Fms. all exhibit a uniform $\sim 185^\circ$ dip direction (Fig. 2). The XYSS and SYSS Fms. have a relatively small dip angle ($\sim 32^\circ$), while the dip angle of the SZG Fm. increases to $\sim 47^\circ$. It is noteworthy that the growth strata (GS) developed in the top part of the SZG Fm. are characterized by the dip of the strata decreasing from $\sim 55^\circ$ to 10° , upwards (Fig. 2).

Using magnetostratigraphy, combined with the results of ostracod (Yang, 1988) and other paleontological analyses (Wang et al., 2007, 2009), Fang et al. (2006) determined the age of the HGZ section to be ~ 17 –5 Ma for the sequence from 120 to 1014 m (Fig. 3a, b). Moreover, the respective ages of the XYSS, SYSS, SZG, QGQ Fms. were determined to be > 17 Ma, ~ 17 –9.8 Ma, ~ 9.8 –5 Ma and $< \sim 5$ Ma (Fig. 3a, b). The bottom age of the XYSS Fm. and the top age of the QGQ Fm. in the western Qaidam Basin were further constrained by magnetostratigraphic dating to 22 Ma (Zhang, 2006) and 2.5 Ma (Luo et al., 2017), respectively.

3. Materials and methods

Sedimentological analyses of the HGZ section include the following:

- (1) Detailed lithological description and observations of bedding

thickness and bedding boundaries recorded in the field. (2) Producing a curve of lithological variations as proposed by Lü et al. (2006). (3) Quantitative analysis of the occurrence of conglomerate and sandstone beds within each 100-m stratigraphic interval using a 20-m moving window, and calculation of sedimentation rates. (4) Collecting a total of 68 representative bulk samples for grain-size analysis to obtain information on the sediment transportation mode (i.e., by traction, saltation or in suspension) of the HGZ section, and thus to characterize the sedimentary dynamics; sample preparation procedures followed those of Lu and An (1997), and the measurements were made using a laser grain-size analyzer (Malvern Mastersizer 2000) at the Key Laboratory of Western China's Environmental Systems, Lanzhou University.

In addition, two sets of seismic profiles across the western margin of the Qaidam Basin provided by the Qinghai Branch of Petro China (see Fig. 1b for their locations) were analyzed to trace the growth strata and deformation history of the study areas. The pre-stack migration of 2-D seismic profiles was calibrated by Normal-moveout and Dip-moveout. Drill-holes (Yue 1, Feng 2 and Gou 4; see Fig. 1b for locations) were used to facilitate the stratigraphic interpretation of the seismic profiles (Fig. 10a, b).

4. Sedimentological analysis of the HGZ section

4.1. Depositional environment of the HGZ section since ~17 Ma

In field, the sedimentary facies of the HGZ section were identified on the basis of color, composition, sedimentary structures, and fossil content (Reading, 1996). The section can be divided into two major intervals based on color representing the predominant grey-green and blue-grey on the basal part (Fig. 2d–f) and predominant light greenish-yellowish grey on the upper part (Fig. 2h–j). These color changes reflect a trend towards the development of a shallow-water depositional environment (Reading, 1996).

The lithology of the HGZ section is primarily composed of three conglomerate sequences, located in the bottom, middle and top parts of the section; a mudstone sequence; and a sandstone sequence (Figs. 2, 3a, c). Based on the magnetostratigraphic age control, the three thick conglomerate layers are dated to ~17–16 Ma, 10 Ma and 5 Ma, respectively (Fig. 3a, b). Two series of strata separated by the second conglomerate layer exhibit distinct sedimentary characteristics. The first, with an age range of 16–10 Ma, consists mainly of calcareous mudstone and mudstone intercalated with thin marl and siltstone or limestone layers (Figs. 2d–f, 3a–c). The second one, with the age range of 10–5 Ma, is dominated by coarse-grained sandstone beds, siltstone and sandy mudstone, intercalated with thin layers of pebbly sandstones or sandy conglomerates (Figs. 2h–j, 3a–c). The method of Lü et al. (2006) was used to provide a graphical representation of the lithological variations: marl or limestone, mudstone, siltstone, sandstone, medium sandstone, coarse sandstone, fine conglomerate, medium conglomerate and coarse conglomerate were assigned values of 1, 2, 3, 4, 5, 6, 7, 8 and 9, respectively, to produce a continuous curve, at a 0.5-m resolution. The results were plotted against depth and they indicate a general upwards-coarsening trend from 17 Ma to 5 Ma (Fig. 3c).

Detailed analysis of the sedimentary structures of the HGZ section by Song et al. (2014) demonstrated that the first and third conglomerate layers are characterized by thick (2–30 m) black-grey breccia beds, with a massive structure, poorly sorted and are matrix supported. The second conglomerate layer has weakly-developed parallel bedding or is massive, poorly sorted and matrix supported with angular gravels with an average particle diameter of 10–50 mm. A wide range of sedimentary textures and structures is developed within the mudstone sequence of the section (16–10 Ma), including parallel bedding, rhythmic bedding and trace fossils in the form of burrows. The sandstone sequences of the section (10–5 Ma) are characterized by parallel bedding, ripple bedding, wavy bedding and ripple structures.

Based on the variations in sediment color, lithology, sedimentary structures and fossil content described above, and sedimentary facies division criteria (Reading, 1996), we conclude that the HGZ section records the following sequence of sedimentary environments: alluvial-fan delta front (17–16 Ma), semi-deep lake (16–11 Ma), fan delta front (11–5 Ma), and alluvial (< 5 Ma). There is a coarse-fine-coarse sequence of sedimentary types and characteristics from the bottom to the top, and in addition a general upward-coarsening succession of lithofacies (Fig. 2, 3a–b, f, h).

In general, the boundary between the traction and saltation components of the sediment grain-size is 2ϕ (250 μm) (Fuller, 1961; Visher, 1969), while the boundary between the saltation and suspension components is 3.3ϕ (100 μm) (Visher, 1969). The results of the grain-size analyses are summarized as follows: (1) The samples from the XYSS Fm. have clear bimodal distributions with peaks centered on 10 μm and 420 μm , (Fig. 3d1), indicating a combination of traction, saltation and suspension transport (Fig. 3e1). The gentle slope of the cumulative frequency curve (on a probability scale) indicates poor sorting and a high energy sedimentary environment. (2) The samples from the lower part of the SYSS Fm. (Fig. 3d2) are unimodal with the peak centered on ~84 μm . The cumulative frequency curve (Fig. 3e2) indicates that particles were mainly transported by saltation and suspension, and a

minor component by rolling; in addition, the steeper slope, compared to the sample from the XYSS Fm., implies better sorting. (3) The samples from the middle-upper part of the SYSS Fm. have a well-defined unimodal distribution (Fig. 3d3), with the mode at 9 μm . The cumulative frequency curves (Fig. 3e3) indicate the dominance of transport in suspension, and the steep slopes suggest a relatively low energy sedimentary environment. (4) The samples from the top part of the SYSS Fm. and the bottom of the SZG Fm. have bimodal distributions with modes of 21 μm and 240 μm (Fig. 3d4). Their cumulative frequency distributions (Fig. 3e4) indicate transport mainly by saltation and in suspension, with a minor rolling component; the shallow slope angles suggest a relatively high energy sedimentary environment. (5) The samples from the SZG Fm. (Fig. 3d5) have a unimodal distribution with modal sizes at 23 μm or 55 μm ; the cumulative frequency distribution curves (Fig. 3e5) indicate transport mainly by saltation and in suspension, with a minor rolling component; the steep slope angles suggest a relatively high energy sedimentary environment. (6) The samples from the top of the SZG Fm. (Fig. 3d6, Fig. 3e6) have similar grain-size characteristics to those from the bottom of the SZG Fm., but with a lower content of coarse grains; they probably deposited in a relatively high energy sedimentary environment. (7) The samples from the QGQ Fm., consisted of agglomerations of coarse particles, were not suitable for grain-size analysis; however, the field characteristics of the QGQ Fm. resembled those of the XYSS Fm. and the dynamics of the sedimentary environment were probably similar. The foregoing observations suggest that the sedimentary environment of the HGZ section became progressively shallower and more energetic from ~17 Ma onwards, and during this interval two 1st-order and seven 2nd-order sequences can be identified, as shown in the Fig. 3f, g. This conclusion is consistent with the changes in the sedimentary environment indicated by the variation in color, lithology, sedimentary structures and fossil content.

In summary, the HGZ section records the following evolutionary sequence of sedimentary environments: alluvial-fan delta front (17–16 Ma), semi-deep lake (16–11 Ma), fan delta front (11–5 Ma), alluvial (< 5 Ma) (Fig. 3h). The fan delta front can be further subdivided into several sub-facies: fan delta-front channel, channel bar, mouth-beyond bar and sheet bar, with increasing water depth (Fig. 3i).

4.2. Variation of the percentage occurrence of conglomerate and sandstone beds

From the detailed lithological description of the HGZ section, we estimated the percentage occurrence of conglomerate and sandstone beds for each 100-m stratigraphic interval, using a 20-m moving window. The results suggest that the distribution of conglomerates are dominant within the age ranges of ~17–16 Ma, ~10–9 Ma and < 5 Ma, and sandstones display peak representation from 9.8–4.8 Ma, with an interval of low representation from 16.5–9.8 Ma (Fig. 4).

4.3. Variations in sedimentation rate (SR)

Variations in SR can be determined from the magnetostratigraphic ages and the thicknesses of the intervening stratigraphic intervals. The SR of the HGZ section (Fig. 5) exhibits an overall upward-increasing trend with two intervals of relatively high values from ~17–16 Ma (11.4 cm/kyr) and 9.8–8.53 Ma (10.27 cm/kyr) and three intervals of relatively low values from 16 to 13.2 Ma (5.19 cm/kyr), 13.2–9.8 Ma (6.14 cm/kyr) and 8.53–4.8 Ma (8.26 cm/kyr).

4.4. Sedimentary provenance of the study area

The provenance of clastic materials, supplied to sedimentary basins by the drainage system, can provide information about tectonic uplift, exhumation and weathering, and the unroofing history of the

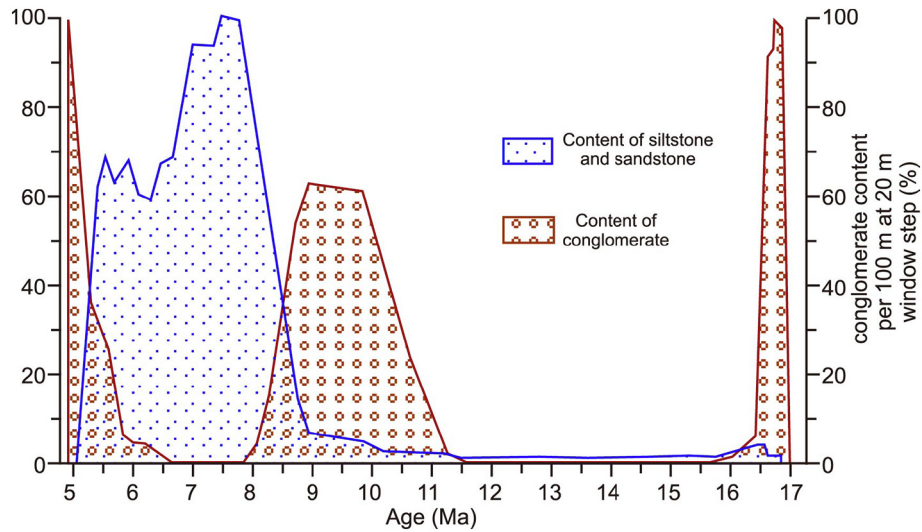


Fig. 4. Variation of the percentage occurrence of conglomerate and sandstone beds in the HGZ section, calculated for each 50-m stratigraphic interval using a 20-m moving window.

surrounding mountains. Various methods have been used to distinguish the provenance of sediments, including analyses of grain composition, heavy minerals, paleocurrent directions, mineralogy, whole-rock geochemistry, as well as radiometric dating and electron microprobe analyses (Weltje and von Eynatten, 2004; Najman, 2006). Zhang et al. (2016a) conducted the analyses of clast composition and paleocurrent directions to constrain the sedimentary provenance of the HGZ section.

The results showed that the composition of the conglomerate beds was relatively uniform, similar to the Proterozoic lithologies of the ATM (Milan and Changcheng Groups); in addition, the paleocurrent directions in the region were mainly southward-oriented, away from the ATR (Fig. 6a, c). Both sets of results suggest that the ATR is the sedimentary source of the HGZ section.

In addition, we analyzed and summarized the results of previous

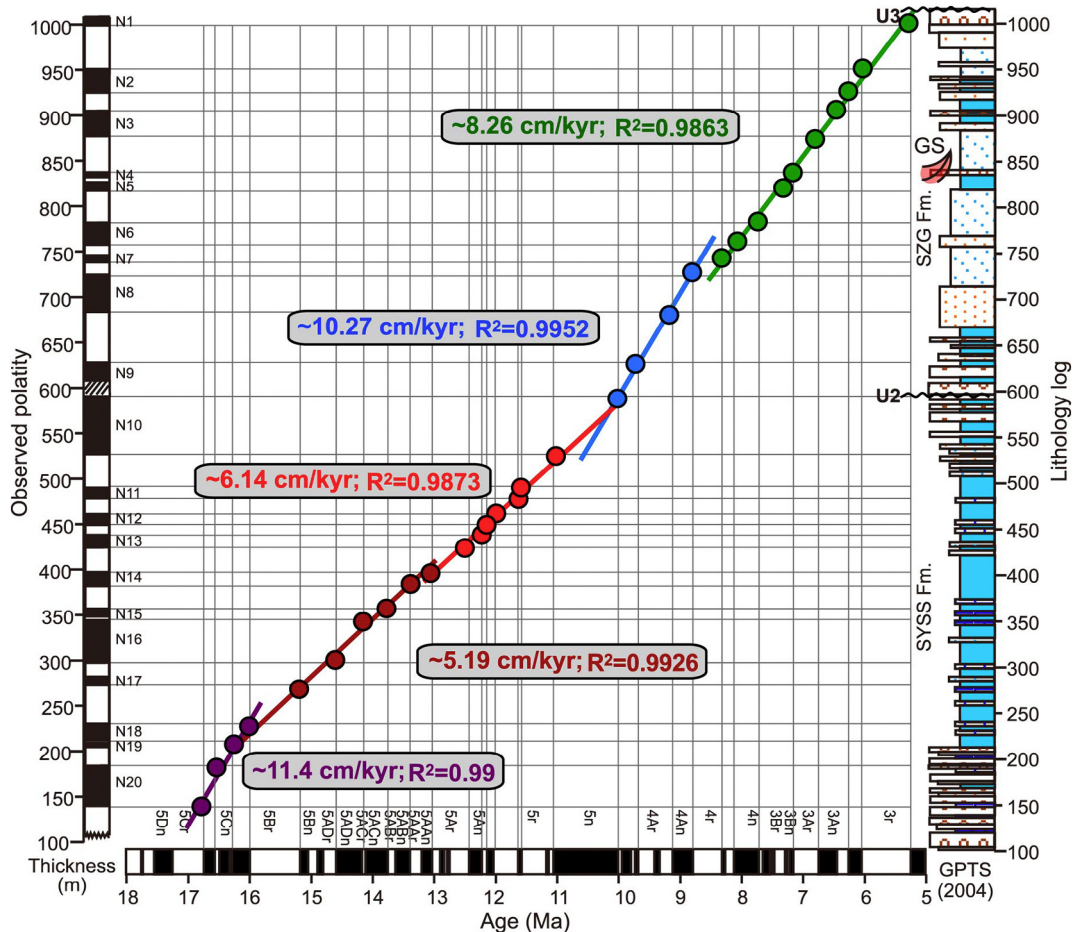


Fig. 5. Stratigraphic thickness as a function of magnetostratigraphic age of the HGZ section, illustrating changes in sedimentation rates.

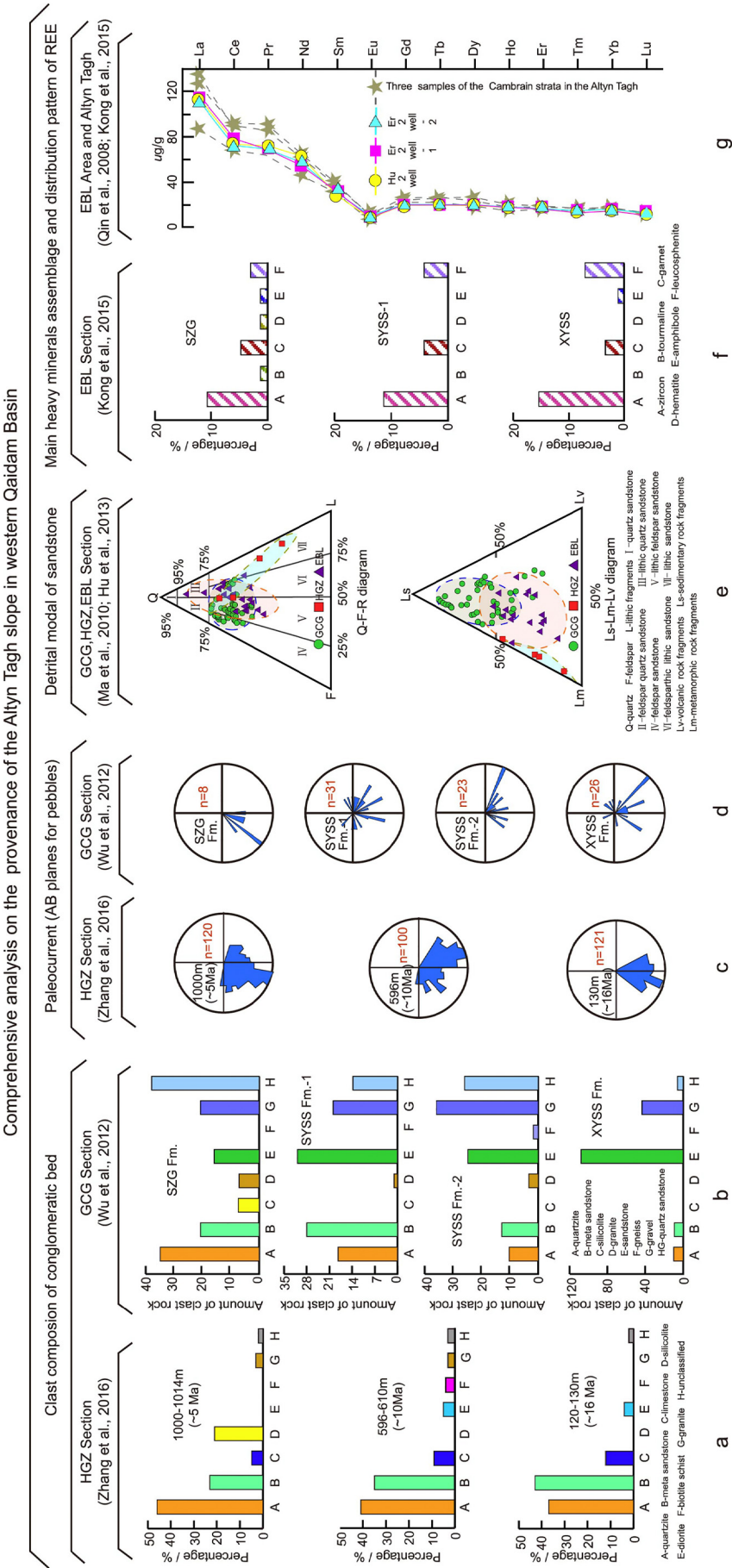


Fig. 6. Results of provenance analysis of the Altyn Tagh slope in the Western Qaidam Basin. Conglomerate components and paleocurrent directions of the GCG and HGZ section are from Wu et al. (2012) and Zhang et al. (2016a). Sand component data for the GCG, HGZ and EBL sections are from Ma et al. (2010) and Hu (2013). Heavy mineral and rare earth element (REE) data for the EBL section are from Kong et al. (2015), and REE data for the Altyn Tagh are from Tan et al. (2008). GCG-Ganchaigou, EBL-Eboliang.

sedimentary provenance studies of another two sections (the Ganchaigou and Eboliang sections nearby the ATR in the western Qaidam Basin, near the HGZ section; see Fig. 1 for locations). Statistical analysis of the components and the composition of the conglomerates shows that the HGZ section (Fig. 6a) has similarities with the gravels of the syndepositional Ganchaigou section which are believed to be derived from the ATM (Fig. 6b). In addition, the modal compositions of the sandstones of the HGZ, Ganchaigou and Eboliang sections are similar, with the clastic material as the major component and the mineral types mainly consisting of lithic feldspar sandstone and feldspathic lithic sandstone (Fig. 6e, top photo), implying that the low maturity of the clastic material in the study area results from the proximal nature of the deposits and their rapid accumulation rate. The distribution diagram of the clastic material in these three sections reveals substantial similarity, consisting mainly of fragments of sedimentary and metamorphic rock, with either a small quantity (or zero) volcanic rock fragments (Fig. 6e, bottom photo). In contrast, the lithology of the ATM, located on the periphery of the three sections, consists mainly of clastic and carbonate rocks, followed by metamorphic rocks, minor intrusive rocks and plagiogranites, with a very small quantity of volcanic material. The major lithologies of the Qimantage Mountains consist of intrusive rocks, granite, minor metamorphic rocks, and clastic and carbonate rocks. The major lithologies of the Sertengshan consist mainly of pre-Triassic strata and Caledonian-Indosinian intermediate and intrusive rocks (GMRBQP, 1991; GMRBXUAR, 1993), suggesting that the projection of the debris components of the sandstones in the three sections is essentially the same as the lithology of the ATM, and that it differs from that of Qimantage Mountain and Sertengshan, which are dominated by intrusive rocks with lesser amounts of clastic and metamorphic rocks. These results also indicate that the ATM is the major sedimentary provenance for the study area. Moreover, the heavy mineral assemblages in the Eboliang (Fig. 6f), and the rare-earth element characteristics, also support a close relationship between the protolith in the ATM and the Neogene deposits, and thus that the ATM is the main provenance of the Neogene deposits in the study area (Tan et al., 2008; Kong et al., 2015). We therefore conclude that the middle-late Miocene deposits of the study areas are probably derived from the ATM.

5. Discussion

5.1. Summary of the stages and processes of paleoenvironmental evolution in the study area

Based on the sedimentary characteristics of the HGZ section, including sedimentary source, lithology, lithofacies, color and sedimentation rates, together with field investigations, we conclude that the HGZ section records five evolutionary stages representing variations in water depth (Fig. 7). The stages are summarized as follows: *Stage 1* (~17–16 Ma). Deposition of a coarse-grained conglomerate-based alluvial facies, with an angular unconformable contact with the underlying Jurassic strata; the SR was rapid. *Stage 2* (16–10 Ma). Fine-grained deposition (e.g., mudstone and marlstone) in a moderately-deep lake or fan-prodelta environment; the SR was relatively low. *Stage 3* (~10–8.53 Ma). Deposition of coarse sediments and a large set of conglomerates in a fan delta front environment; the SR was variable compared to the preceding stage and an unconformity exists at ~10 Ma. *Stage 4* (8.53–5 Ma). The sedimentary environment was principally a fan delta front, with a decreasing conglomerate content and a high sandstone content; the SR decreased slightly. *Stage 5* (< 5 Ma). Deposition of a coarse-grained conglomerate-based alluvial facies with an angular unconformable contact with the underlying strata.

To summarize the evolution of sedimentary environments in the study area since the late Cenozoic, data from boreholes, field observations and previous studies near to the HGZ section were used to establish structural-sedimentary cross sections both parallel and

perpendicular (Fig. 8) to the ATF. The sections parallel to the ATF (Fig. 7) include the Qi-31 borehole and the XCG section in the western Qaidam Basin (on the southern side of the ATR); the YTBK and DB sections in the Xorkol Basin in the hinterland of the ATR; and the MR and JGNSY sections in the southeastern Tarim Basin (on the northern side of the ATR) (see Fig. 1 for site locations). These sections are readily correlated and they record a similar process of sedimentary environmental evolution. The paleo-water-depth in the hinterland and northern side of the ATR was shallower comparing to the southern side of the range. These sections also indicate a deeper water environment with finer sediments in *stage 2* (~16–10 Ma) than in *stage 1* (~17–16 Ma) (Fig. 7). The sections perpendicular to the ATF (Fig. 8) exhibit a gradual basinward deepening of the water depth and a basinward increase in sedimentary thickness, indicating the gradual migration of the depocenter from west to east during the late Cenozoic. More specifically, there was a progressive shallowing of the paleo-water-depth of the HGZ and XLS structural belt in the western Piedmont region, while that of the NYS structural belt of the central region remained stable, and that of the KTMLK structural belt in the eastern region, progressively deepened. Thus, these results reveal two spatio-temporal patterns of sedimentary environmental evolution in the study area since the late Cenozoic: progressive shallowing of the water depth horizontally, and basinward migration of the depocenter perpendicularly.

5.2. Factors controlling the variation in the sedimentary characteristics of the HGZ area

The variations in the sedimentary characteristics of the NE Tibetan Plateau and the surrounding region have been ascribed to tectonic uplift (e.g., Zheng et al., 2000; Fang et al., 2005, 2007; Yue et al., 2004b; Charreau et al., 2006; Ritts et al., 2008; Lu and Xiong, 2009; Zhuang et al., 2011a; Wu et al., 2012; Li et al., 2014; Chang et al., 2015; Lu et al., 2015; Fang et al., 2016) or to climate change (e.g., Zhang et al., 2001; Molnar, 2004). However, it is difficult to differentiate the effects of tectonic activity and climate change from sedimentary characteristics alone (Molnar and England, 1990). It has been assumed that sedimentary characteristics are mainly controlled by tectonics during tectonically active intervals. In addition, during tectonically quiet intervals, a stable climate would maintain an equilibrium geomorphological state, while pronounced climate changes on a sub-tectonic timescale would significantly affect the sedimentary characteristics (Zhang et al., 2001; Molnar, 2004). We try to distinguish the relative effects of tectonics and climate on the late Cenozoic evolution of the sedimentary environment in the HGZ area in the next section.

5.2.1. Climate change records from the HGZ section and surrounding area

We used 10 high-resolution paleoclimate records from the HGZ section (Fig. 9b, c) (Song et al., 2014) and surrounding areas (Fig. 9d, e, f, g, h) (Wang et al., 1999; Miao et al., 2011, 2016a, 2016b; Zhuang et al., 2011b), and the adjacent Tarim and Junggar Basins (Fig. 9h, i) (Tang et al., 2011; Zhang and Sun, 2011), as well as deep-sea sediment records (Fig. 9j, k) (Zachos et al., 2001; de Boer et al., 2010), to assess the effects of climate change on the sedimentary characteristics (Fig. 9). The concentration of soluble SO_4^{2-} and Cl^- increased continuously from ~17 Ma and reached on average higher values at ~5.0 Ma (Fig. 9b, c) (Song et al., 2014), which was believed to reflect increased salinity in response to the long-term gradual aridification of the Qaidam Basin (Song et al., 2014). The sedimentary facies, biomarkers, and stable isotopes from the XLS area, adjacent to the HGZ section (Fig. 1b, c), all revealed a gradual drying and cooling trend in the study area during the middle-late Miocene (Jian et al., 2014). Pollen and spore assemblages from the western Qaidam Basin indicate progressive aridification since the Mid-Miocene (Fig. 9d, e, g) (e.g., Wang et al., 1999; Miao et al., 2011, 2016a, 2016b). Similarly, pollen records from the

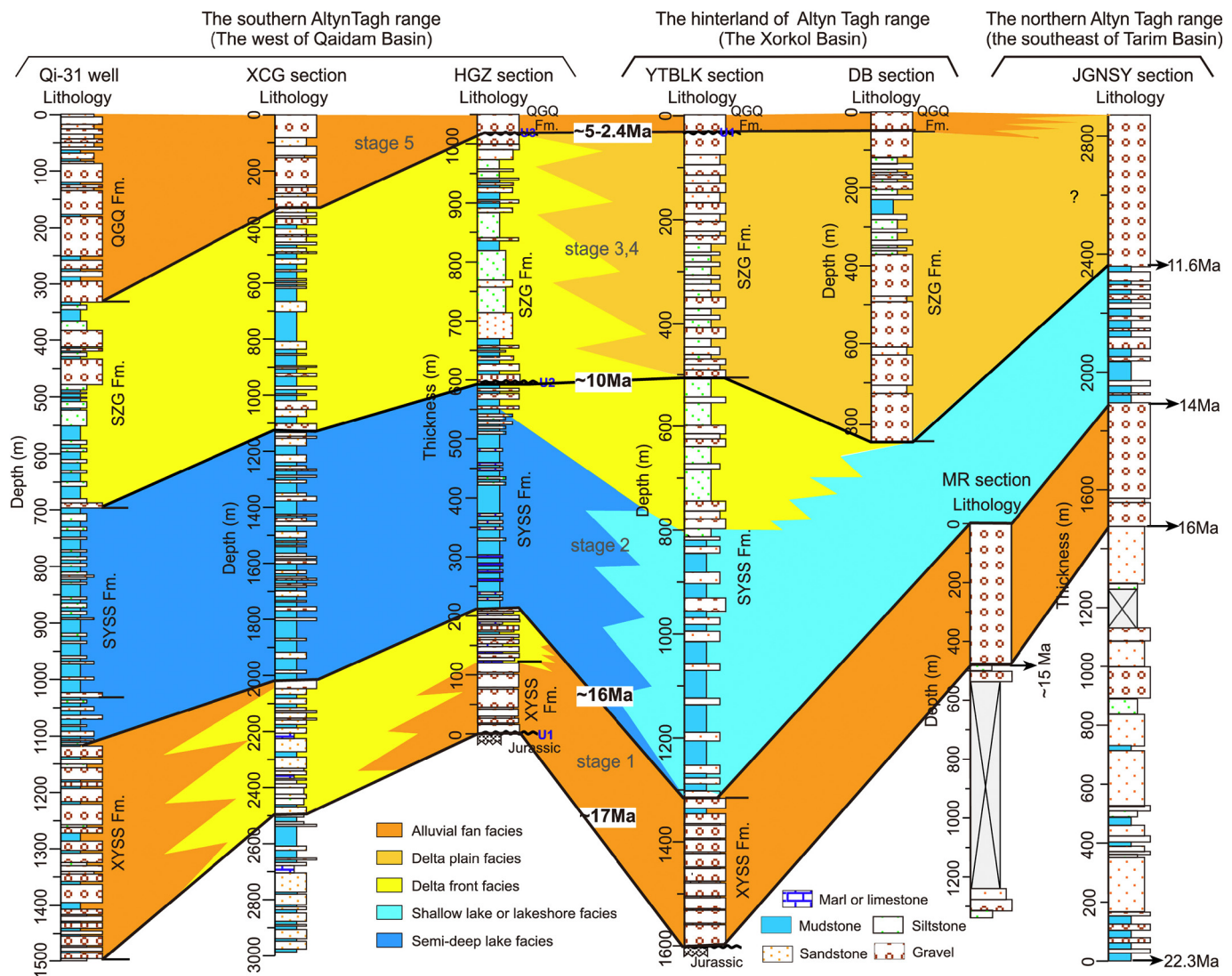


Fig. 7. Sediment facies and lithologies along a cross section parallel to the Altyn Tagh fault. Data sources for the sections are as follows: MR (Ritts et al., 2008); JGNSY (Lu et al., 2014); Qi-31 (Qinghai Oilfield Company of the China's National Petroleum Corporation); XCG, HGZ, DB (this study). Locations of the sections and boreholes are shown in Fig. 1.

Kuchetawu section, north Tarim Basin (Fig. 9h) (Zhang and Sun, 2011) and the Jingouhe section in the southern Junggar Basin (Fig. 9i) (Tang et al., 2011), indicate a gradual drying and cooling trend since the Miocene. The chemical weathering evaluation (Jian et al., 2013) and stable isotope records (Fig. 9f) (Zhuang et al., 2011b) also shows the increased aridity of the Qaidam Basin since ~12 Ma. The similar paleoclimatic trends recorded by terrestrial sedimentary records during 17–5 Ma, temperature simulations with a 1-D ice-sheet model (Fig. 9j) (de Boer et al., 2010) and the global deep-sea oxygen isotope record (Fig. 9k) (Zachos et al., 2001) both suggest an overall cooling trend since the Middle Miocene Climatic Optimum. Various humidity proxies show that overall the Qaidam Basin and surrounding regions of the NE Tibetan Plateau experienced a gradual drying trend since ~17 Ma (especially at ~14–12 Ma). Furthermore, the previous studies suggested that only pronounced climate changes on a sub-tectonic timescale would significantly affect the sedimentary characteristics, such as a change from a warm and humid climate to a cold and dry climate (Zhang et al., 2001; Molnar, 2004). The paleoclimatic records summarized in Fig. 9 suggest only a relatively minor change from a dry middle Miocene climate to drier conditions in the late Miocene, which is out of phase with the changes in the sedimentary characteristics, including the SR (Fig. 9a). Thus, we conclude that climatic change was

not the major driver of the observed changes in the sedimentary characteristics of the study area.

5.2.2. Local and regional tectonic records from the study area

We also analyzed seismostratigraphic data for the study area to explore the relationship between the sedimentary records and tectonic activity (Fig. 10). Growth strata (GS), which are deposited against the flanks or on top of growing structures, are often used to reveal the structural kinematic processes of fault-related folding (Suppe et al., 1997). Much work has been done to decipher the relationship between the deposition of syntectonic sediments and the fault-induced tilt of strata (e.g., Storti and Poblet, 1997; Rafini and Mercier, 2002). The details of tectonic deformation are directly recorded by the GS and can be quantified by the growth triangles of it (e.g., Suppe et al., 1992). A formula for estimating the growth rate of the GS (GR) was proposed by Li et al. (2014):

$$GR = \delta(\theta)/\delta(t) \quad (1)$$

where $\delta(\theta)$ and $\delta(t)$ are the growth angle difference and the growth interval, respectively. $\delta(\theta)$ will be relatively constant with time to form a set of recognizable GS if folding deformation maintains a constant rate (Fig. 10c1). An acceleration of folding and thrusting will cause a

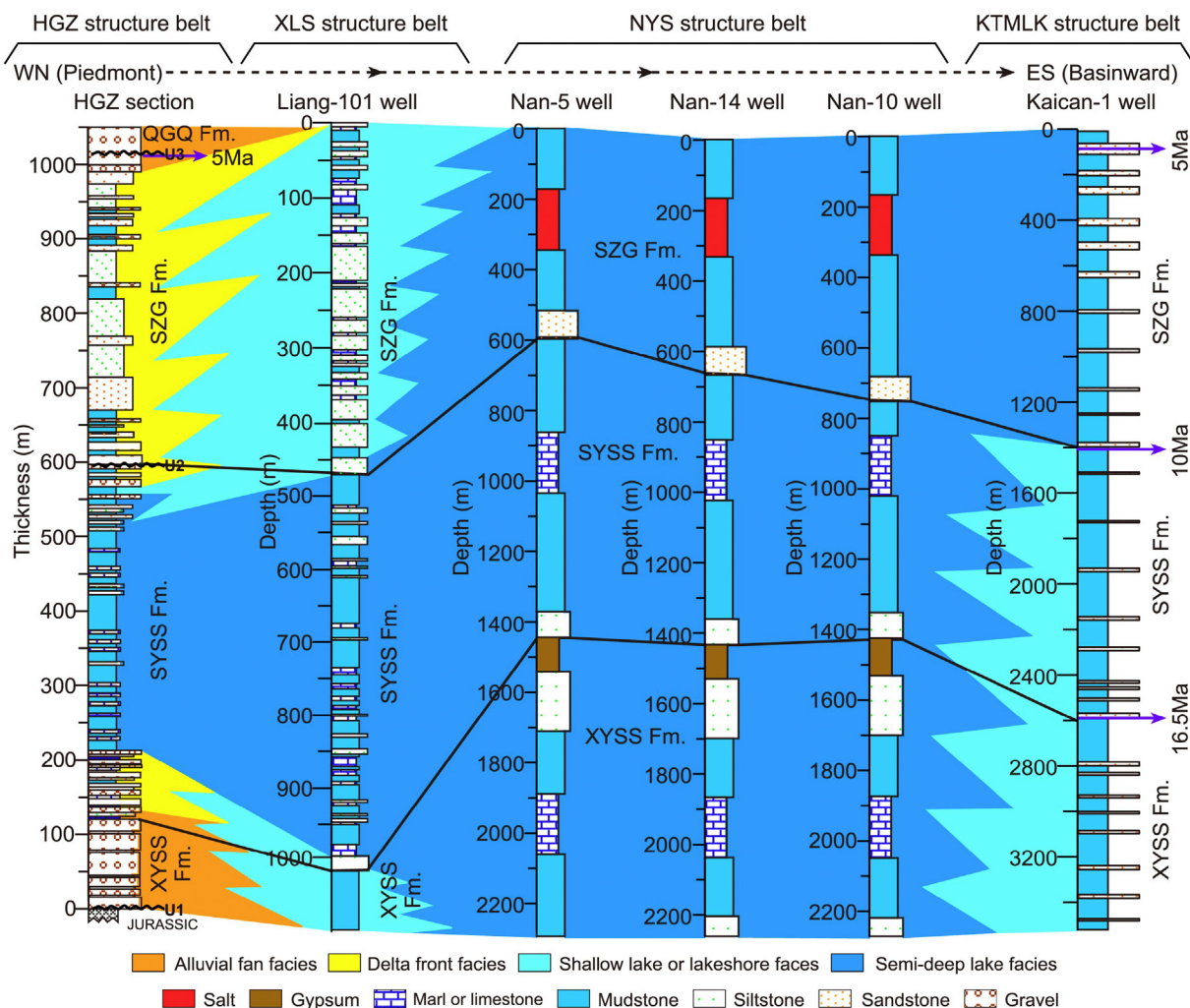


Fig. 8. Sediment facies and lithologies along a cross section perpendicular to the Altyn Tagh fault. Data sources for the sections are as follows: HGZ (this study); Kaican-1 (Miao et al., 2016a); Liang-101, Nan-5, Nan-14 and Nan-10 (Qinghai Oilfield Company of China's National Petroleum Corporation). The locations of the sections and boreholes are shown in Fig. 1.

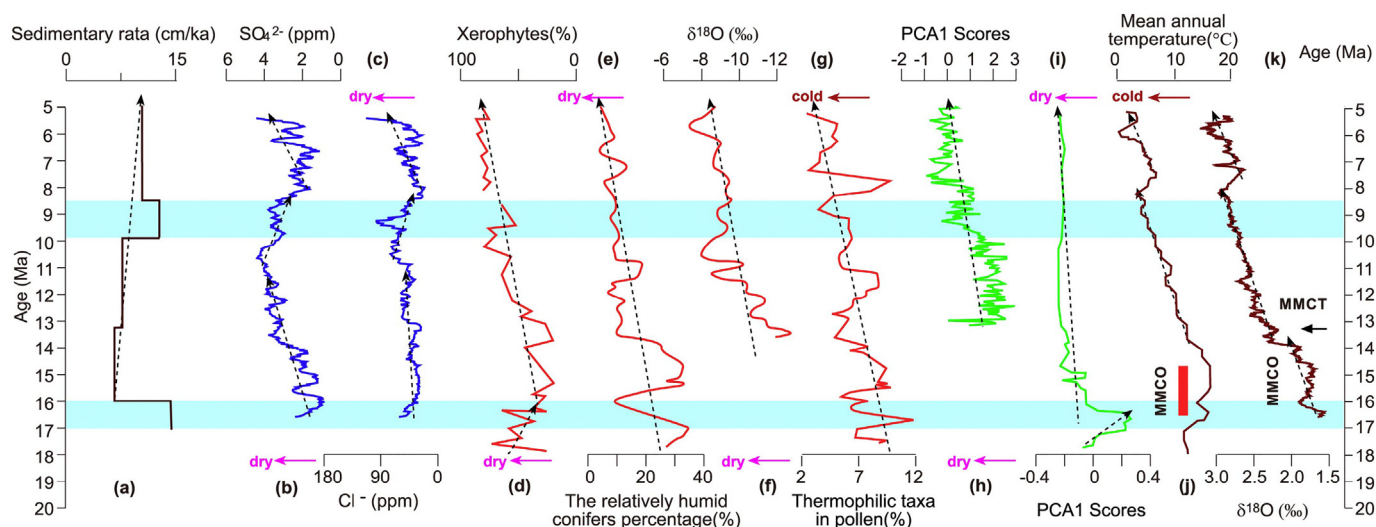


Fig. 9. Variations in the sedimentation rate of the HGZ section and comparison with paleoclimatic records for the study area and surrounding regions (modified from Zhang et al., 2016a).

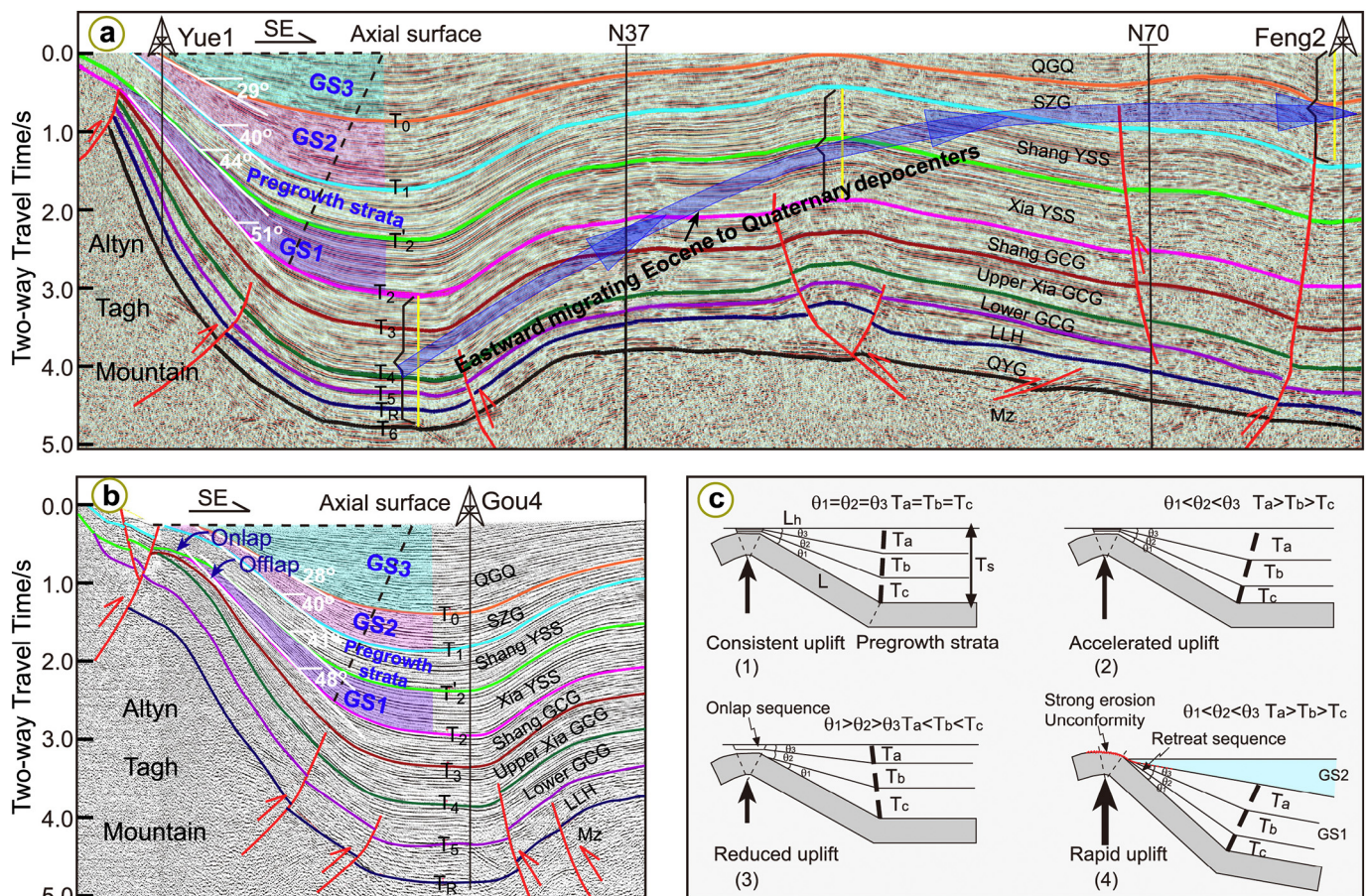


Fig. 10. (a, b) Seismostratigraphy along the western margin of the Qaidam Basin and eastern slope of the Altyn Tagh, showing the occurrence of growth strata during the late Cenozoic (see Fig. 1b for their location). (c) Schematic diagrams showing the relationship between uplift rate and growth strata development and the associated unconformity and stratigraphic sequence (Li et al., 2014). QGQ - Qigequan Fm., SZG - Shizigou Fm., Shang YSS - Shang Youshashan Fm., Xia YSS - Xia Youshashan Fm., Shang GCG - Shang Ganchaigou Fm., Upper Xia GCG - Upper Xia Ganchaigou Fm., Lower Xia GCG - Lower Xia Ganchaigou Fm., LLH - Lulehe Fm., QYG - Quanyagou Fm.

decrease in the thickness of sediments deposited on the upslope part or on the top of the fold, as well as an increased corresponding growth angle (Fig. 10c2). When the folding and thrusting are too rapid, it lacks the deposition at the head of the fold and results erosion. The folding and erosion rates may enhance either parallel or angular unconformity which later leads to the formation of a retreat depositional sequence (Fig. 10c4) and vice-versa will produce an onlapping stratigraphic sequence (Fig. 10c3).

Thus, observations of GS and stratigraphic dip allow us to determine the timing and rate of specific tectonic deformation events in the study area. Magnetostratigraphic results for the HGZ section, together with previously published paleomagnetic data and fossil assemblages from the western Qaidam Basin (Zhang, 2006; Zhang et al., 2013; Luo et al., 2017), enable us to constrain the ages of the syn-tectonic GR. Two seismic profiles across the western Qaidam Basin (Fig. 10a, b; see Fig. 1b for locations) clearly demonstrate that three large sets of GS structure, GS1 to GS3, developed since the late Cenozoic. GS1 was formed at the XYSS Fm. (~22–16.5 Ma), where the dips of the a-section and b-section changed from 51° to 44° and from 48° to 41°, respectively (Figs. 10a, b, 11a), with the same growth rate ($GR = 1.27^\circ/\text{Ma}$) during this stage. GS2 developed at the SZG Fm. (10–2.5 Ma), and is consistent with observations of outcrop in the HGZ section (Fig. 2); the corresponding dip angles changed from 40° to 29° ($GR = 1.47^\circ/\text{Ma}$) for the a-section and from 40° to 28° ($GR = 1.60^\circ/\text{Ma}$) for the b-section (Fig. 11a). The youngest unit affected by GS3 developed at the QGQ Fm. at ~2.5 Ma. GS3 exhibits an abrupt change in dip angle from 29° (a-section) or from 28° (b-section) to 0° (Fig. 11A); the GR of GS3 was

estimated as $11.60^\circ/\text{Ma}$ and $11.20^\circ/\text{Ma}$, respectively. Therefore, the development of GS1, GS2 and GS3, as indicated by increases in GR, demonstrate that the study area experienced roughly three episodes of tectonic activity since 22 Ma, with accelerating folding and upheaval (Fig. 11A). These tectonic episodes are temporally well-correlated with the sedimentary characteristics of the three conglomerate sequences, and with the high SR phase and the general upwards-coarsening trend in the lithology of the HGZ section. In addition, Fig. 10a reveals that the Cenozoic sedimentation pattern of the western Qaidam Basin was largely controlled by the successive and gradual eastward migration of depocenters since the Eocene, which may indicate the gradual uplift of the ATR. This inference is consistent with the basinward deepening of the water depth recorded by the cross-section perpendicular to the ATF (Fig. 8). Furthermore, from Fig. 10b, an angular unconformity can be identified between the XYSS Fm. and SYSS Fm. (~17 Ma) which is consistent with the records (unconformity U1) of the HGZ section. The fact that the Altyn Tagh Mountains were onlapped by massive sedimentary deposits can also be identified from Fig. 10b, indicating that the Qaidam Basin was rapidly expanding westwards, and that the deposition of the SYSS Fm. gradually onlapped the erosional uplifting belt, over older strata formed in different periods (Fig. 10b).

To quantify the tectonic evolution and shortening history, we carried out the balanced cross-section restoration of the seismic profile shown in Fig. 10a (details of cross section restoration and balancing will be described in a forthcoming publication). The result shows that the total crustal deformation shortening of the a-section is ~5.31 km, with a total shortening ratio of 20.49% (Fig. 11B). The shortening ratio

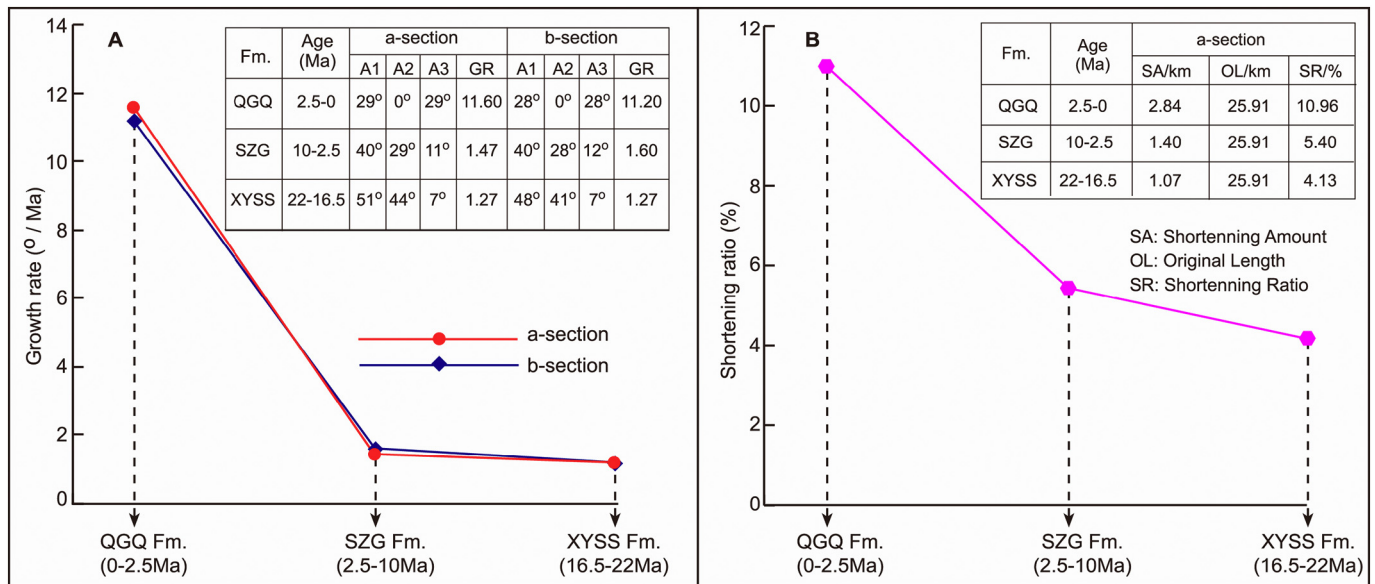


Fig. 11. (A) Variations in growth rate calculated from a re-interpretation of seismic profiles a and b (see Fig. 10a and b, respectively), (B) variation of the shortening ratio calculated from the balanced cross-section restoration of Fig. 10a.

generally reveals an increasing trend since 23 Ma: 4.13% between 23 and 16.5 Ma, 5.40% between 16.5 and 10 Ma, and 10.96% between 2.6 and 0 Ma (Fig. 11B), representing three episodes of tectonic activity since 23 Ma along with accelerating crustal shortening in the study area (Fig. 11B). This is also consistent with the GS and GR results (Figs. 10 and 11A).

In addition, three stages of tectonic uplift of the HGZ area are revealed. For example, three unconformities, U1 to U3, accompanied by thick conglomerate deposits, can be identified in the HGZ section (Fig. 3). The first angular unconformity (U1) lies at the top of XYSS Fm (~17 Ma), U2 is located at the boundary of the SZG Fm. and SYSS Fm. (~10 Ma), and U3 is located at the boundary of QGG Fm. and SZG Fm. (< 5 Ma). An upward-coarsening succession with increasing sedimentation rate in the HGZ section suggests a decreasing distance from the sediment source to the areas of deposition, because of tectonic changes, which would have led to an increase in the sediment grain-size and rate of deposition, even with the same amount of runoff.

The results of various other studies also indicate that late Cenozoic uplift in the western Qaidam Basin and surrounding mountains occurred in three stages: (i) A late Oligocene-middle Miocene tectonic event (~23–16 Ma) was shown by the SHRIMP zircon U–Pb dating derived from clasts in the Xorkol and Yitunbulake Basin (Zhang et al., 2016b), apatite fission-track studies from the ATM (Ge et al., 1998; Ritts et al., 2008), sedimentary records in the surrounding basins of the ATR (e.g., Yue et al., 2001, 2004a; Fang et al., 2007; Ritts et al., 2008; Wang et al., 2010; Wu et al., 2012; Chang et al., 2015), structural analysis in the ATF or Qaidam Basin (Cowgill et al., 2003; Xiao et al., 2013; Cheng et al., 2015a, 2015b; Mao et al., 2016; Zhao et al., 2016), and tectonic rotation in the Janggalsay section of the Eastern Tarim Basin (Lu et al., 2014). (ii) Late Miocene (~10–8 Ma) tectonic uplift was revealed by apatite fission-track data analysis (e.g., Ge et al., 1998; Jolivet et al., 1999, 2001; Wan et al., 2001; Chen et al., 2006; Zhang et al., 2012b; Liu et al., 2017), $^{40}\text{Ar}/^{39}\text{Ar}$ dating (Liu et al., 2007), sedimentologic analyses in the nearby basin (Chen et al., 2005; Song et al., 2014), and various other methods (Li et al., 2006; Yuan et al., 2006; Miao et al., 2016b; Zhang et al., 2016a). (iii) A late Pliocene-Quaternary (3.6–0 Ma) tectonic event was revealed by the interpretation of satellite images and a seismic profile (Pan et al., 2015), and by the sedimentology of sites adjacent to the ATR (Li et al., 2006; Chang et al., 2012; Lu et al., 2015).

It can be concluded from the foregoing evidence that three tectonic

uplift events occurred in the western Qaidam Basin and ATR during the late Cenozoic, and are closely matched with the timing of abrupt changes in sedimentary characteristics near the HGZ section: at ~17–16 Ma, 10 Ma and < 5 Ma. Thus, we conclude that the variations in the sedimentary record documented by the HGZ section were a direct response to the tectonic evolution of the study area.

5.3. Conceptual model linking changes in the sedimentary records and tectonic activity in the ATR

At present, there are three main evolutionary models regarding the temporal relationships between rapid uplift of the ATM and left-lateral strike-slip motion of the ATF. For example, Yin et al. (2002) argued for synchronous rapid uplift of the ATM and fast left-lateral strike-slip motion of the ATF since as early as ~49 Ma. Yue et al. (2004a, 2004b) and Ritts et al. (2004, 2008) proposed that fast left-lateral strike-slip motion of the ATF occurred between the late Oligocene and the Mid-Miocene and that subsequently the ATM began to uplift rapidly. Wu et al. (2012) proposed that rapid uplift of the ATM occurred from 36 to 15 Ma, with subsequent fast left-lateral strike-slip motion of the ATF since ~15 Ma. Although these studies provide an opportunity to understand the tectonic evolution history of the ATR, the results are mutually conflicting and they are mainly focused on the early Cenozoic, especially earlier than 15 Ma. We thus propose a possible conceptual model based on the foregoing evidences to elucidate the relationship between sedimentary records and tectonic activity of the ATR in the study area since the late Cenozoic. Compared with the more intense tectonic activity after 22 Ma, the possible tectonic activity before 22 Ma (e.g., Jolivet et al., 2001; Yin et al., 2002; Liu et al., 2007; Wu et al., 2012; Zhao et al., 2016) may not have caused a significant height difference of the terrain or the topographic relief between the southwestern Qaidam Basin and the ATR (Fig. 12A), where a large sedimentary depocenter continuously received sediments supplied by eastward-flowing drainage in the western Qaidam Basin (Fig. 10a).

5.3.1. ~22–16 Ma

During this interval, and especially at ~ > 17–16 Ma, the ATR was subjected to major stresses resulting from the India-Asia collision. At that time, the vector component (strike slip stress) of the principal stress in the areas parallel to ATR was relatively weak, leading to a weak strike-slip movement (Fig. 12B). The vector component (uplift

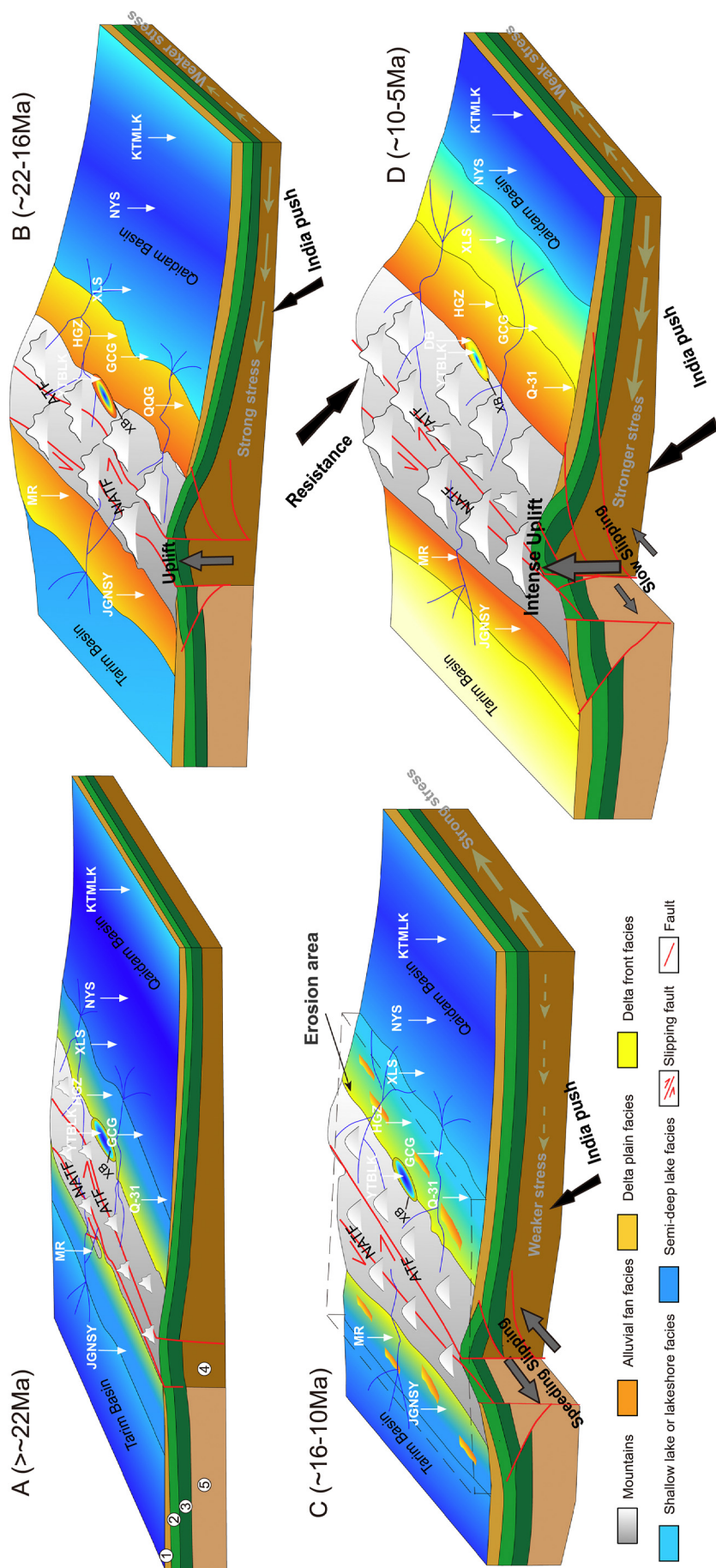


Fig. 12. Conceptual model illustrating the relationship between tectonic and topographic evolution of the Altyn Tagh range and the spatiotemporal variation of sedimentary characteristics in the HGZ area in the western Qaidam Basin since the late Cenozoic. NATF: north Altyn Tagh fault; XB: Xorkol Basin; 1: sediments deposited since the late Cenozoic; 2: Mesozoic and early Cenozoic rocks; 3: Paleozoic rocks and the Proterozoic basement; 4: relatively elastic crust of the Qaidam Basin; 6: rigid crust of the Taim Basin. Note that the thicknesses of the layers are not to scale.

stress) perpendicular to the ATR was relatively strong, although hindered by the Tarim Block, leading to continuously increasing uplift stress, and hence to a further thickening of the crust in the area and uplift of the mountains (Fig. 12B). This resulted in the shedding of coarse alluvial conglomerate-based sediments into piedmont areas (Fig. 7). Consequently, the supply of sediments from the source to the study area was rapid and the SR was high (Fig. 5) during this stage. At the same time, basement fault activity was strengthened and expanded basinward, leading to uplift of the basin-mountain junction. A regional unconformity (U1) (Fig. 3a; Wang et al., 2010) and the GS were thus formed, and there was a basinward migration of the depocenter (Fig. 10a).

5.3.2. ~16–10 Ma

The Indian Plate moved continuously northwards, and the absorption rate of the uplift stress perpendicular to the ATR may have decreased because of the increasing total amount of stress. The convergence of stress at the strike-slip component parallel to the ATR would lead to the initiation of the rapid left-lateral and strike-slip fault of the Altyn Tagh (Fig. 12C), which was also supported by Wu et al. (2012) and Zhao et al. (2016), and by recent new paleomagnetic evidence (Li et al., 2017). Due to the release and rapid migration of the potential uplift energy to a horizontal strike slip motion, the basement of the ATR subsided strongly and the scope and amplitude of the mountain uplift decreased. In this situation, the relatively lower uplift rate compared to the rate of subsidence or weathering and denudation in local regions would facilitate the change of early uplifting and erosional areas to a relatively subsiding area receiving sediments (Fig. 12C). This change in accommodation would have caused the sedimentary strata to prograde and overlap gradually towards the mountains (Fig. 10b). At the same time, the dominant strike slip motion of the ATR would favor subsidence of the basement or form a pull-apart/down-faulted basin, thus leading to the relatively finer sediments (mainly fine-grained mudstone and marlstone) in the western part of the Qaidam Basin during this stage compared to the previous stage (Figs. 7, 8), and a lower SR (Fig. 5).

5.3.3. ~10–5 Ma

As the Indian Plate thrust progressively northwards, the constant eastward strike-slip movement of the left-lateral and strike-slip fault of Altyn Tagh was progressively hindered by the Alashan Block, which resulted in the main tectonic stress being transformed from strike slip stress, parallel to the ATR, to uplift stress perpendicular to the ATR (Fig. 12D). Therefore, the extensive and intense uplift was due to the tectonic activity of the ATR and a strong supply of sediment from the nearer source area (Fig. 12D). Consequently, piedmont areas accumulated coarse-grained sediments and the SR increased accordingly (Figs. 5, 7), and a strong tectonic deformation in the basin caused by large basinward expansion of the basement fault forms the GS and unconformity (U2) (Figs. 3a, 10). This caused the depocenter to migrate rapidly eastwards, and there was a shallowing of the water depth near the HGZ and XLS areas, which were closer to the piedmont. In contrast, the water depth in the KTMK area deepened and the sedimentary thickness increased (Fig. 8).

Our new conceptual model for the tectonic evolution of the ATR again supports the gradually accelerated eastward extrusion of the Tibetan Plateau driven by the India-Asia collision during the late Cenozoic. However, the foregoing interpretation is based primarily on the observed changes in sedimentary characteristics of the study areas during the late Cenozoic, and further studies are needed to substantiate our results before reaching a final conclusion about our conceptual model and the relative roles of tectonics and climate change in determining the late Cenozoic sedimentary characteristics of the region.

6. Conclusions

We performed detailed sedimentological analyses of the late Cenozoic HGZ section in the western Qaidam Basin, combined with the analysis of data from nearby boreholes and sections in the surrounding region. In addition, we have integrated the findings with the results of detailed tectonic field investigations and seismostratigraphic analysis of the region. Our conclusions are as follows:

1) During the late Cenozoic, the water-depth of the HGZ area experienced a progressive shallowing, and there was an upward-coarsening of the lithofacies and eastward migration of the depocenter. The sedimentary characteristics of the study area exhibit three major stages of evolution: $\sim > 17$ –16 Ma, 10 Ma and < 5 Ma.

2) The timing of the three stages is strongly related to the development of three unconformities and GS recorded by high-resolution seismic reflection profiles in the study area. In addition, based on a summary and analysis of the previously published records of climatic change and tectonic activity in the study area, we conclude that changes in the sedimentary records of the HGZ area were a direct response to tectonic activity, and climate change played only a subordinate role.

3) Combined with a comprehensive provenance analysis, we suggest the evolution of the sedimentary characteristics of the study area may reflect the major tectonic responses of the western Qaidam Basin to the tectonic evolution of the ATR, at $\sim > 17$ –16 Ma, ~ 16 –10 Ma and ~ 10 Ma. We propose a possible model related respectively to tectonic uplift, fast strike-slip motion, and intense uplift, during these stages, which needs to be assessed by future studies.

Acknowledgments

This paper benefited significantly from constructive suggestions from Jean-Philippe Avouac, Feng Cheng and other anonymous reviewers. This work was co-supported by the Strategic Priority Research Program of Chinese Academy of Sciences (grant XDA20070201), National Natural Science Foundation (NSFC grants. 41502172; 41571200; 41620104002), Project funded by China Postdoctoral Science Foundation (grant 2015M581181) and Natural Science Foundation of Shandong Province (grant ZR2015JL015). Special thanks go to the Qinghai Oilfield Company of China National Petroleum Corporation for providing us with borehole and seismic profiles. Many thanks are due to D.L. Liu, L.P. Yu, Z.G. Zhang, F.L. Wu, J.B. Zan and J., Bao for their valuable field and laboratory assistance. The authors are grateful to Prof. Jan Bloemendal and Mr. Dhan Bahadur Khatri for improving the English.

Appendix A. Supplementary data

Supplementary data to this article can be found online at <https://doi.org/10.1016/j.tecto.2018.04.021>.

References

- An, Z.S., Kutzbach, J.E., Prell, W.L., Porter, S.C., 2001. Evolution of Asian monsoons and phased uplift of the Himalaya-Tibetan plateau since Late Miocene times. *Nature* 411, 62–66.
- Argand, E., 1924. La tectonique de l'Asie. *Rep. Sess.-Int. Geol. Congr.* 13, 170–372.
- Armijo, R., Tapponnier, P., Han, T., 1989. Late Cenozoic right-lateral strike-slip faulting in southern Tibet. *J. Geophys. Res.* 94 (B3), 2787–2838.
- Avouac, J., Tapponnier, P., 1993. Kinematic model of active deformation in central Asia. *Geophys. Res. Lett.* 20, 895–898.
- de Boer, B., van de Wal, R.S.W., Bintanja, R., Lourens, L.J., Tuenter, E., 2010. Cenozoic global ice-volume and temperature simulations with 1-D ice-sheet models forced by benthic $\delta^{18}O$ records. *Ann. Glaciol.* 51, 23–33.
- Bush, M.A., Saylor, J.E., Horton, B.K., Nie, J.S., 2016. Growth of the Qaidam Basin during Cenozoic exhumation in the northern Tibetan Plateau: inferences from depositional patterns and multiproxy detrital provenance signatures. *Lithosphere* 8, 58–82.
- Chang, H., Ao, H., An, Z.S., Fang, X.M., Song, Y.G., Qiang, X.K., 2012. Magnetostratigraphy of the Suerkuli Basin indicates Pliocene (3.2 Ma) activity of the

- middle Altyn Tagh Fault, northern Tibetan Plateau. *J. Asian Earth Sci.* 44, 169–175.
- Chang, H., Li, L.Y., Qiang, X.K., Garzzone, C.N., Pullen, A., An, Z.S., 2015. Magnetostratigraphy of Cenozoic deposits in the western Qaidam Basin and its implication for the surface uplift of the northeastern margin of the Tibetan Plateau. *Earth Planet. Sci. Lett.* 430, 271–283.
- Charreau, J., Gilder, S., Chen, Y., Dominguez, S., Avouac, J.-P., Sen, S., Jolivet, M., Li, Y.A., Wang, W.M., 2006. Magnetostratigraphy of the Yaha section, Tarim Basin (China): 11 Ma acceleration in erosion and uplift of the Tian Shan Mountains. *Geology* 34 (3), 181–184 (2006).
- Chen, Z.L., Liu, J., Sun, Z.M., Wang, X.F., Pei, J.L., Gong, H.L., 2005. Cenozoic erosional history of the Altyn Tagh mountains inferred from the sedimentary record of the foreland basin. *Geol. Bull. China* 24 (4), 302–308 (in Chinese).
- Chen, Z.L., Gong, H.L., Li, L., Wang, X.F., Chen, B.L., Chen, X.H., 2006. Cenozoic uplifting and exhumation process of the Altyn Tagh mountains. *Earth Sci. Front.* 13 (4), 91–102 (in Chinese).
- Cheng, F., Jolivet, M., Dupont-Nivet, G., Wang, L., Yu, X.J., Guo, Z.J., 2015a. Lateral extrusion along the Altyn Tagh Fault, Qilian Shan (NE Tibet): insight from a 3D crustal budget. *Terra Nova* 27, 416–425.
- Cheng, F., Guo, Z.J., Jenkins, H.S., Fu, S.T., Cheng, X., 2015b. Initial rupture and displacement on the Altyn Tagh fault, northern Tibetan Plateau: constraints based on residual Mesozoic to Cenozoic strata in the western Qaidam Basin. *Geosphere* 11, 921–942.
- Cheng, F., Jolivet, M., Fu, S.T., Zhang, C.H., Zhang, Q.Q., Guo, Z.J., 2016a. Large-scale displacement along the Altyn Tagh Fault (North Tibet) since its Eocene initiation: insight from detrital zircon U-Pb geochronology and subsurface data. *Tectonophysics* 677, 261–279.
- Cheng, F., Fu, S.T., Jolivet, M., Zhang, C.H., Guo, Z.J., 2016b. Source to sink relation between the Eastern Kunlun Range and the Qaidam Basin, northern Tibetan Plateau, during the Cenozoic. *Geol. Soc. Am. Bull.* 128, 258–283.
- Cheng, F., Jolivet, M., Hallot, E., Zhang, D.W., Zhang, C.H., Guo, Z.J., 2017. Tectono-magmatic rejuvenation of the Qaidam craton, northern Tibet. *Gondwana Res.* 49, 248–263.
- Cowgill, E., Yin, A., Harrison, T.M., Wang, X.F., 2003. Reconstruction of the Altyn Tagh fault based on U-Pb geochronology: role of back thrusts, mantle sutures, and heterogeneous crustal strength in forming the Tibetan Plateau. *J. Geophys. Res.* 108, 2346.
- CSBS (Chinese State Bureau of Seismology), 1992. The Altyn Tagh Active Fault System. Seismology Publishing House, Beijing, pp. 1–319 (in Chinese).
- Darby, B., Ritts, B.D., Yue, Y.J., Meng, Q.R., 2005. Did the Altyn Tagh fault extend beyond the Tibetan Plateau? *Earth Planet. Sci. Lett.* 240, 425–435.
- Delville, N., Arnaud, N., Montel, J.M., Roger, F., Brunel, M., Tapponnier, P., Sobel, E., 2001. Paleozoic to Cenozoic deformation along the Altyn Tagh fault in the Altun Shan massif area, eastern Qilian Shan, northeastern Tibet, China. *Geol. Soc. Am. Mem.* 194, 269–292.
- England, P., Houseman, G.A., 1986. Finite strain calculations of continental deformation, 2, comparison with the India–Asia collision zone. *J. Geophys. Res.* 91, 3664–3676.
- Fang, X.M., Yan, M.D., Van der Voo, R., Rea, D.K., Song, C.H., Pares, J.M., Nie, J.S., Gao, J.P., Dai, S., 2005. Late Cenozoic deformation and uplift of the NE Tibetan Plateau: evidence from high-resolution magnetostratigraphy of the Guide Basin, Qinghai Province. *China. Geol. Soc. Am. Bull.* 117, 1208–1225.
- Fang, X.M., Gao, J.P., Zhang, W.L., Wang, Y.D., Liu, D.L., 2006. Detailed Evolution of Qiqeguan-Yueyashan Tectonics in the Front of Altyn Tagh and Western Qaidam Basin and Selection of Prospective Targets. Report of Academy 2005-Kantan-JSFWHT-23, Qinghai Oil Company. pp. 1–122 (in Chinese).
- Fang, X.M., Zhang, W.L., Meng, Q.Q., Gao, J.J., Wang, X.M., King, J., Song, C.H., Dai, S., Miao, Y.F., 2007. High-resolution magnetostratigraphy of the Neogene Huaitoutala section in the eastern Qaidam Basin on the NE Tibetan Plateau, Qinghai Province, China and its implication on tectonic uplift of the NE Tibetan Plateau. *Earth Planet. Sci. Lett.* 258 (1), 293–306.
- Fang, X.M., Liu, D.L., Song, C.H., Dai, S., Meng, Q.Q., 2013. Oligocene slow and Miocene–Quaternary rapid deformation and uplift of the Yumu Shan and North Qilian Shan: evidence from high-resolution magnetostratigraphy and tectonosedimentology. *Geol. Soc. Lond., Spec. Publ.* 373 (1), 149–171.
- Fang, X.M., Wang, J.Y., Zhang, W.L., Zan, J.B., Song, C.H., Yan, M.D., Appel, E., Zhang, T., Wu, F.L., Yang, Y.B., Lu, Y., 2016. Tectonosedimentary evolution model of an intracontinental flexural (foreland) basin for paleoclimatic research. *Glob. Planet. Chang.* 145, 78–97.
- Fuller, A., 1961. Size characteristics of shallow marine sands from Cape of Good Hope, South Africa. *J. Sediment. Petrol.* 31 (2), 256–261.
- Ge, X.H., Zhang, M.S., Liu, Y.J., Ye, H.W., Shi, C.D., 1998. Scientific problems and thought for research of the Altun fault. *Geoscience* 12 (3), 295–301 (in Chinese).
- Geological and Mineral Resources Bureau of Qinghai Province (GMRBQP), 1991. Regional Geology of Qinghai Province. Geological Publishing House, Beijing, pp. 605 (in Chinese).
- Geological and Mineral Resources Bureau of Xinjiang Uygur Autonomous Region (GMRBXUAR), 1993. Regional Geology of Xinjiang Uygur Autonomous Region. Geological Publishing House, Beijing, pp. 762 (in Chinese).
- Hu, X., 2013. The Characteristics of Cenozoic Sedimentary and Provenance Analysis in the Northern Qaidam Basin (Master thesis). Chengdu University of Technology, Chengdu, pp. 30–49 (in Chinese).
- Huang, H.C., Huang, Q.H., Ma, Y.S., 1996. Geology of Qaidam and Petroleum Prediction. Geological Publ. House, Beijing, pp. 1–257 (in Chinese).
- Jian, X., Guan, P., Zhang, W., Feng, F., 2013. Geochemistry of Mesozoic and Cenozoic sediments in the northern Qaidam basin, northeastern Tibetan Plateau: implications for provenance and weathering. *Chem. Geol.* 360, 74–88.
- Jian, X., Guan, P., Fu, S.T., Zhang, D.W., Zhang, W., Zhang, Y.S., 2014. Miocene sedimentary environment and climate change in the northwestern Qaidam basin, northeastern Tibetan Plateau: facies, biomarker and stable isotopic evidences. *Palaeogeogr. Palaeoclimatol. Palaeoecol.* 414, 320–331.
- Jolivet, M., Roger, F., Arnaud, N., Brunel, M., Tapponnier, P., Seward, D., 1999. Histoire de l'exhumation de l'Altun Shan: indications sur l'âge de la subduction du bloc du Tarim sous le système de l'Altyn Tagh (Nord Tibet). *C. R. Acad. Sci. Ser. IIA Earth Planet. Sci.* 329, 749–755.
- Jolivet, M., Brunel, M., Seward, D., Xu, Z.Q., Yang, J.S., Roger, F., Tapponnier, P., Malavieille, J., Arnaud, N., Wu, C., 2001. Mesozoic and Cenozoic tectonics of the northern edge of the Tibetan plateau: fission-track constraints. *Tectonophysics* 343, 111–134.
- Kong, H., Zhao, J., Hou, Z.S., Si, D., Zai, Z.W., Ma, J.Y., Shen, Y.S., 2015. Provenance analysis and sedimentary environment evolution of the Neogene in Eboliang III structure of Qaidam Basin. *J. Palaeogeogr.* 17 (1), 51–62 (2015). (in Chinese).
- Li, H.B., Yang, J.S., Xu, Z.Q., Sun, Z.M., Tapponnier, P., van der Woerd, J., Meriaux, A.S., 2006. The constraint of the Altyn Tagh fault system to the growth and rise of the northern Tibetan plateau. *Earth Sci. Front.* 13, 59–79 (in Chinese).
- Li, J.J., Fang, X.M., Song, C.H., Pan, B.T., Ma, Y.Z., Yan, M.D., 2014. Late Miocene–Quaternary rapid stepwise uplift of the NE Tibetan Plateau and its effects on climatic and environmental changes. *Quat. Res.* 81 (3), 400–423.
- Li, B.S., Yan, M.D., Zhang, W.L., Fang, X.M., Meng, Q.Q., Zan, J.B., Chen, Y., Zhang, D.W., Yang, Y.P., Guan, C., 2017. New paleomagnetic constraints on middle Miocene strike-slip faulting along the middle Altyn Tagh fault. *J. Geophys. Res. Solid Earth* 122, 4106–4122.
- Liu, Y., Neubauer, F., Genser, J., Ge, X.H., Takasu, A.S., Yuan, H., Chang, L.H., Li, W.M., 2007. Geochronology of the initiation and displacement of the Altyn Strike-Slip Fault, western China. *J. Asian Earth Sci.* 29, 243–252.
- Liu, X.D., Sun, H., Miao, Y.F., Dong, B.W., Yin, Z.Y., 2015. Impacts of uplift of northern Tibetan Plateau and formation of Asian inland deserts on regional climate and environment. *Quat. Sci. Rev.* 116, 1–14.
- Liu, D.L., Li, H.B., Sun, Z.M., Pan, J.W., Wang, M., Wang, H., Luce Chevalier, M., 2017. AFT dating constrains the Cenozoic uplift of the Qimen Tagh Mountains, Northeast Tibetan Plateau, comparison with LA-ICPMS zircon U–Pb ages. *Gondwana Res.* 41, 438–450.
- Lu, H.Y., An, Z.S., 1997. Experimental study on the influence of different pretreatment procedures on the particle-size measurement of loess sediments. *Chin. Sci. Bull.* 42, 2535–2538.
- Lu, H.J., Xiong, S.F., 2009. Magnetostratigraphy of the Dahonggou section, northern Qaidam Basin and its bearing on Cenozoic tectonic evolution of the Qilian Shan and Altyn Tagh Fault. *Earth Planet. Sci. Lett.* 288, 539–550.
- Lü, H.H., Xia, Z.G., Jiang, B., Ren, M., Li, Y.L., 2006. Application of mathematical geology methods to analysis of the sedimentary facies of sandstone reservoir: an example of the reservoir of the Neogene in Huatugou Oilfield, Qaidam Basin. *Acta Sci. Nat. Univ. Pekin.* 42 (4), 462–469 (in Chinese).
- Lu, H.J., Wang, E.Q., Meng, K., 2014. Paleomagnetism and anisotropy of magnetic susceptibility of the Tertiary Janggalsay section (southeast Tarim basin): implications for Miocene tectonic evolution of the Altyn Tagh Range. *Tectonophysics* 618, 67–78.
- Lu, Y., Fang, X.M., Appel, E., Wang, J.Y., Herb, C., Han, W.X., Wu, F.L., Song, C.H., 2015. A 7.3–1.6 Ma grain size record of interaction between anticline uplift and climate change in the western Qaidam Basin, NE Tibetan Plateau. *Sediment. Geol.* 319, 40–51.
- Luo, Z., Su, Q.D., Wang, Z., Heermance, R.V., Garzzone, C., Li, M., Ren, X.P., Song, Y.G., Nie, J.S., 2017. Orbital forcing of Plio-Pleistocene climate variation in a Qaidam Basin lake based on paleomagnetic and evaporite mineralogical analysis. *Palaeogeogr. Palaeoclimatol. Palaeoecol.* <http://dx.doi.org/10.1016/j.palaeo.2017.09.022>.
- Ma, X., Yi, H.S., Xia, G.Q., 2010. Cenozoic sedimentary transformation event record by detrital components in western Qaidam Basin, Qinghai, China. *Geol. Bull. China* 29 (9), 1294–1303 (in Chinese).
- Mao, L.G., Xiao, A.C., Zhang, H.W., Wu, Z.K., Wang, L., Shen, Y., Wu, L., 2016. Structural deformation pattern within the NW Qaidam Basin in the Cenozoic era and its tectonic implications. *Tectonophysics* 687, 78–93.
- Meng, Q., Fang, X., 2008. Cenozoic tectonic development of the Qaidam Basin in the northeastern Tibetan Plateau. *Geol. Soc. Am. Spec. Pap.* 444, 1–24.
- Métivier, F., Gaudemer, Y., Tapponnier, P., Meyer, B., 1998. Northeastward growth of the Tibet plateau deduced from balanced reconstruction of two depositional areas: the Qaidam and Hexi Corridor basins, China. *Tectonics* 17, 823–842.
- Miao, Y.F., Fang, X.M., Herrmann, M., Wu, F.L., Liu, D.L., 2011. Miocene pollen record of KC-1 core in the Qaidam Basin, NE Tibetan Plateau and implications for evolution of the East Asian monsoon. *Palaeogeogr. Palaeoclimatol. Palaeoecol.* 299 (1), 30–38.
- Miao, Y.F., Fang, X.M., Liu, Y.S., Yan, X.L., Li, S.Y., Xia, W.M., 2016a. Late Cenozoic pollen concentration in the western Qaidam Basin, northern Tibetan Plateau, and its significance for paleoclimate and tectonics. *Rev. Palaeobot. Palynol.* 231, 14–22.
- Miao, Y.F., Song, C.H., Fang, X.M., Meng, Q.Q., Zhang, P., Wu, F.L., Yan, X.L., 2016b. Late Cenozoic genus *Fupingopollenites* development and its implications for the Asian summer monsoon evolution. *Gondwana Res.* 29 (1), 320–333.
- Molnar, P., 2004. Late Cenozoic increase in accumulation rates of terrestrial sediment: how might climate change have affected erosion rates? *Annu. Rev. Earth Planet. Sci.* 32 (12), 67–89 (2004).
- Molnar, P., England, P., 1990. Late Cenozoic uplift of mountain ranges and global climate change: chicken or egg? *Nature* 346 (6279), 29–34 (1990).
- Molnar, P., Tapponnier, P., 1975. Cenozoic tectonics of Asia: effects of a continental collision. *Science* 189, 419–426.
- Molnar, P., England, P., Martinod, J., 1993. Mantle dynamics, uplift of the Tibetan Plateau, and the Indian monsoon. *Rev. Geophys.* 31, 357–396. <http://dx.doi.org/10.1029/93RG02030>.
- Najman, Y., 2006. The detrital record of orogenesis: a review of approaches and

- techniques used in the Himalayan sedimentary basins. *Earth Sci. Rev.* 74, 1–72.
- Pan, J.W., Li, H.B., Sun, Z.M., Liu, D.L., Wu, C., Yu, C.Q., 2015. Tectonic responses in the Qaidam basin induced by Cenozoic activities of the Altyn Tagh fault. *Acta Petrol. Sin.* 31 (12), 3701–3712 (in Chinese).
- Rafini, S., Mercier, E., 2002. Forward modeling of foreland basins progressive unconformities. *Sediment. Geol.* 146, 75–89.
- Raymo, M., Ruddiman, W.F., 1988. Froelich P N. Influence of late Cenozoic mountain building on ocean geochemical cycles. *Geology* 16 (7), 649–653.
- Reading, H., 1996. *Sedimentary Environments: Processes, Facies and Stratigraphy*. Blackwell, Oxford, pp. 53–68.
- Ritts, B., Yue, Y.J., Graham, S.A., 2004. Oligocene-Miocene tectonics and sedimentation along the Altyn Tagh Fault, northern Tibetan Plateau: analysis of the Xorkol, Subei, and Aksay basins. *J. Geol.* 112, 207–229.
- Ritts, B., Yue, Y.J., Graham, S.A., Sobel, E.R., Abbink, O.A., Stockli, D., 2008. From sea level to high elevation in 15 million years: uplift history of the northern Tibetan Plateau margin in the Altun Shan. *Am. J. Sci.* 308, 657–678.
- Ruddiman, W., Kutzbach, J.E., 1989. Forcing of the late Cenozoic uplift northern hemisphere climate by plateau uplift in the Southern Asia and American West. *J. Geophys. Res.* 94, 18409–18427.
- Searle, M., 1996. Geological evidence against large-scale pre-Holocene offsets along the Karakoram Fault: implications for the limited extrusion of the Tibetan plateau. *Tectonics* 15, 171–186.
- Searle, M., Elliott, J., Phillips, R., Chung, S.L., 2011. Crustal-lithospheric structure and continental extrusion of Tibet. *J. Geol. Soc.* 168, 633–672.
- Sobel, E., Arnaud, N., Jolivet, M., Ritts, B.D., Brunel, M., 2001. Jurassic to Cenozoic exhumation history of the Altyn Tagh range, Northwest China, constrained by 40Ar/39Ar and apatite fission track thermochronology. *Geol. Soc. Am. Mem.* 194, 247–267.
- Song, C.H., Hu, S.H., Han, W.X., Zhang, T., Fang, X.M., Gao, J.P., Wu, F.L., 2014. Middle Miocene to earliest Pliocene sedimentological and geochemical records of climate change in the western Qaidam Basin on the NE Tibetan Plateau. *Palaeogeogr. Palaeoclimatol. Palaeoecol.* 395, 67–76.
- Storti, F., Poblet, J., 1997. Growth stratal architectures associated to decollement folds and fault-propagation folds. Inferences on fold kinematics. *Tectonophysics* 282 (1–4), 353–373.
- Suppe, J., Chou, G.T., Hook, S.C., 1992. Rate of folding and faulting determined from growth strata. In: McClay, K.R. (Ed.), *Thrust Tectonics*. Springer, Netherlands, pp. 105–121.
- Suppe, J., Sábát, F., Munoz, J.A., Poblet, J., Roca, E., Vergés, J., 1997. Bed-by-bed fold growth by kink-band migration: Sant Llorenç de Morunys, eastern Pyrenees. *J. Struct. Geol.* 19 (3–4), 443–461.
- Tan, X., Xia, B., Li, C.Q., Li, J., Lu, Q.P., Xu, H., Zhou, F.S., Hu, G.A., Li, Q., 2008. Geochemical characteristics and tectonic setting of Precambrian granitic gneiss in the western segment of Altyn Tagh Tectonic Belt. *Geoscience* 22 (1), 34–44 (in Chinese).
- Tang, Z.H., Ding, Z.L., White, P.D., Dong, X.X., Ji, J.L., Jiang, H.C., Luo, P., Wang, X., 2011. Late Cenozoic central Asian drying inferred from a palynological record from the northern Tian Shan. *Earth Planet. Sci. Lett.* 302, 439–447.
- Tapponnier, P., Peltzer, G., Armijo, R., 1986. On the mechanics of the collision between India and Asia. *Geol. Soc. Lond., Spec. Publ.* 19, 113–157.
- Tapponnier, P., Xu, Z.Q., Roger, F., Meyer, B., Arnaud, N., Wittlinger, G., Yang, J.S., 2001. Oblique stepwise rise and growth of the Tibet Plateau. *Science* 294, 1671–1677.
- Visher, G., 1969. Grain size distributions and depositional processes. *J. Sediment. Petrol.* 39 (3), 1074–1106.
- Wan, J.L., Wang, Y., Li, Q., Wang, F., Wang, E.C., 2001. FT evidence of northern Altyn uplift in Late-Cenozoic. *Bull. Mineral. Petrol. Geochim.* 20, 222–224 (in Chinese).
- Wang, E.Q., 1997. Displacement and timing along the northern strand of the Altyn Tagh fault zone, northern Tibet. *Earth Planet. Sci. Lett.* 150, 55–64.
- Wang, J., Wang, Y.J., Liu, Z.C., Li, J.Q., Xi, P., 1999. Cenozoic environmental evolution of the Qaidam Basin and its implications for the uplift of the Tibetan Plateau and the drying of the central Asia. *Palaeogeogr. Palaeoclimatol. Palaeoecol.* 152, 37–47.
- Wang, Y., Zhang, X., Wang, E., Zhang, J., Li, Q., Sun, G., 2005. 40Ar/39Ar thermochronological evidence for formation and Mesozoic evolution of the northern-central segment of the Altyn Tagh fault system in the northern Tibetan Plateau. *Geol. Soc. Am. Bull.* 117, 1336–1346.
- Wang, E.Q., Xu, F.Y., Zhou, J.X., Wan, J., Burchfiel, B.C., 2006. Eastward migration of the Qaidam basin and its implications for Cenozoic evolution of the Altyn Tagh fault and associated river systems. *Geol. Soc. Am. Bull.* 118, 349–365.
- Wang, X.M., Qiu, Z.D., Li, Q., Wang, B.Y., Qiu, Z.X., William, R.D., Xie, G.P., Xie, J.Y., Deng, T., Takeuchi, G.T., Tseng, Z.J., Chang, M.M., Liu, J., Wang, Y., Biasatti, D., Sun, Z.C., Fang, X.M., Meng, Q.Q., 2007. Vertebrate paleontology, biostratigraphy, geochronology, and paleoenvironment of Qaidam Basin in northern Tibetan Plateau. *Palaeogeogr. Palaeoclimatol. Palaeoecol.* 254 (3), 363–385.
- Wang, C.S., Zhao, X.X., Liu, Z.F., Lippert, P.C., Graham, S.A., Coe, R.S., Yi, H.S., Zhu, L.D., Liu, S., Li, Y.L., 2008. Constraints on the early uplift history of the Tibetan Plateau. *Proc. Natl. Acad. Sci.* 105 (13), 4987–4992.
- Wang, X.M., Xie, G.P., Dong, W., 2009. A new species of crown-antlered deer *Stephanocemas* (Artiodactyla, Cervidae) from the middle Miocene of Qaidam Basin, northern Tibetan Plateau, China, and a preliminary evaluation of its phylogeny. *Zool. J. Linnean Soc.* 156 (3), 680–695.
- Wang, L., Xiao, A.C., Gong, Q.L., Liu, D., Wu, L., Zhou, S.P., Shen, Z.Y., Lou, Q.Q., Sun, X.W., 2010. The unconformity in Miocene sequence of the western Qaidam Basin and its tectonic significance. *Sci. China Earth Sci.* 53, 1126–1133.
- Wang, C.S., Dai, J.G., Zhao, X.X., Li, Y.L., Graham, S.A., He, D.F., Ran, B., Meng, J., 2014. Outward-growth of the Tibetan Plateau during the Cenozoic: a review. *Tectonophysics* 621, 1–43.
- Wang, Y.D., Zheng, J.J., Zheng, Y.W., Liu, X.W., Sun, G.Q., 2015. Paleocene-Early Eocene uplift of the Altyn Tagh Mountain: evidence from detrital zircon fission track analysis and seismic sections in the northwestern Qaidam basin. *J. Geophys. Res. Solid Earth* 120 (12), 8534–8550.
- Weltje, G., von Eynatten, H., 2004. Quantitative provenance analysis of sediments: review and outlook. *Sediment. Geol.* 171, 1–11.
- Wittlinger, G., Tapponnier, P., Poupinet, G., Mei, J., Danian, S., Herquel, G., Masson, F., 1998. Tomographic evidence for localized lithospheric shear along the Altyn Tagh fault. *Science* 282, 74–76.
- Wu, L., Xiao, A.C., Yang, S.F., Wang, L.Q., Mao, L.G., Wang, L., Dong, Y.P., Xu, B., 2012. Two stage evolution of the Altyn Tagh Fault during the Cenozoic: new insight from provenance analysis of a geological section in NW Qaidam Basin, NW China. *Terra Nova* 24, 387–395.
- Xia, W., Zhang, N., Yuan, X.P., Fan, L.S., Zhang, B.S., 2001. Cenozoic Qaidam basin, China: a stronger tectonic inversed, extensional rifted basin. *AAPG Bull.* 85 (4), 715–736.
- Xiao, A.C., Wu, L., Li, H.G., Wang, L.Q., 2013. Tectonic processes of the Cenozoic Altyn Tagh Fault and its coupling with the Qaidam Basin, NW China. *Acta Petrol. Sin.* 29 (8), 2826–2836 (in Chinese).
- Xu, X., Gao, R., Dong, S.W., Wang, H.Y., Guo, X.Y., 2017. Lateral extrusion of the northern Tibetan Plateau interpreted from seismic images, potential field data, and structural analysis of the eastern Kunlun fault. *Tectonophysics* 696–697, 88–98.
- Yang, F., 1988. Distribution of the brackish-salt water ostracod in northwestern Qinghai Plateau and its geological significance. In: Hanai, T., Ikeya, T., Ishizaki, K. (Eds.), *Evolutionary Biology of Ostracoda*. Proc. 9th Int. Symp. Ostracoda, Shizuoka, Japan, pp. 519–530.
- Yin, A., Rumelhart, P.E., Butler, R., Cowgill, E., Harrison, T.M., Foster, D.A., Ingersoll, R.V., Qing, Z., Zhou, X.Q., Wang, X.F., Hanson, A., Raza, A., 2002. Tectonic history of the Altyn Tagh fault system in northern Tibet inferred from Cenozoic sedimentation. *Geol. Soc. Am. Bull.* 114, 1257–1295.
- Yin, A., Dang, Y.Q., Wang, L.C., Jiang, W.M., Zhou, S.P., Chen, X.H., Gehrels, G.E., McRivette, M.W., 2008a. Cenozoic tectonic evolution of Qaidam basin and its surrounding regions (part 1): the southern Qilian Shan-Nan Shan thrust belt and northern Qaidam basin. *Geol. Soc. Am. Bull.* 120, 813–846.
- Yin, A., Dang, Y.Q., Zhang, M., Chen, X.H., McRivette, M.W., 2008b. Cenozoic tectonic evolution of the Qaidam basin and its surrounding regions (part 3): structural geology, sedimentation, and regional tectonic reconstruction. *Geol. Soc. Am. Bull.* 120, 847–876.
- Yuan, S., Liu, Y.J., Ge, X.H., Ren, S.M., Wu, D.G., Li, W.M., 2006. Advance in study of mesozoic-cenozoic uplift history of the Altyn mountains. *Glob. Geol.* 25 (2), 164–171 (in Chinese).
- Yue, Y.J., Liou, J.G., 1999. Two-stage evolution model for the Altyn Tagh fault, China. *Geology* 27, 227–230.
- Yue, Y.J., Ritts, B.D., Graham, S.A., 2001. Initiation and long-term slip history of the Altyn Tagh Fault. *Int. Geol. Rev.* 43, 1087–1093.
- Yue, Y.J., Ritts, B.D., Graham, S.A., Wooden, J.L., Gehrels, G.E., Zhang, Z., 2004a. Slowing extrusion tectonics: lowered estimate of post-Early Miocene slip rate for the Altyn Tagh fault. *Earth Planet. Sci. Lett.* 217, 111–122.
- Yue, Y.J., Ritts, B.D., Hanson, A.D., Graham, S.A., 2004b. Sedimentary evidence against large strike-slip translation on the Northern Altyn Tagh fault, NW China. *Earth Planet. Sci. Lett.* 228, 311–323.
- Yue, Y.J., Graham, S.A., Ritts, B.D., Wooden, J.L., 2005. Detrital zircon provenance evidence for large-scale extrusion along the Altyn Tagh fault. *Tectonophysics* 406, 165–178.
- Zachos, J., Pagani, M., Sloan, L., Thomas, E., Billups, K., 2001. Trends, rhythms, and aberrations in global climate 65 Ma to present. *Science* 292 (5517), 686–693.
- Zhang, W.L., 2006. The High Precise Cenozoic Magnetostratigraphy of the Qaidam Basin and Uplift of the Northern Tibetan Plateau (Doctoral dissertation). Lanzhou University, Lanzhou, pp. 1–105 (in Chinese).
- Zhang, Z.Q., Sun, J.M., 2011. Palynological evidence for Neogene environmental change in the foreland basin of the southern Tianshan range, northwestern China. *Glob. Planet. Chang.* 75, 56–66.
- Zhang, P.Z., Molnar, P., Downs, W.R., 2001. Increased sedimentation rates and grain sizes 2–4 Myr ago due to the influence of climate change on erosion rates. *Nature* 410 (6831), 891–897.
- Zhang, C., Wang, Y., Li, Q., Wang, X.M., Deng, T., Tseng, Z.J., Takeuchi, G.T., Xie, G.P., Xu, Y.F., 2012a. Diets and environments of late Cenozoic mammals in the Qaidam Basin, Tibetan Plateau: evidence from stable isotopes. *Earth Planet. Sci. Lett.* 333–334, 70–82.
- Zhang, Z.C., Guo, Z.J., Li, J.F., Tang, W.H., 2012b. Mesozoic and Cenozoic uplift-denudation along the Altyn Tagh fault, Northwestern China: constraints from apatite fission track data. *Quat. Sci.* 32, 499–509 (in Chinese).
- Zhang, W.L., Fang, X.M., Song, C.H., Appel, E., Yan, M.D., Wang, Y.D., 2013. Late Neogene magnetostratigraphy in the western Qaidam Basin (NE Tibetan Plateau) and its constraints on active tectonic uplift and progressive evolution of growth strata. *Tectonophysics* 599, 107–116.
- Zhang, T., Han, W.X., Fang, X.M., Zhang, W.L., Song, C.H., Yan, M.D., 2016a. Intensified tectonic deformation and uplift of the Altyn Tagh range recorded by rock magnetism and growth strata studies of the western Qaidam Basin, NE Tibetan Plateau. *Glob. Planet. Chang.* 137, 54–68.
- Zhang, Z.G., Nie, J.S., Fang, X.M., 2016b. Provenance analysis reveals mountain uplift in the midsection of the Altyn Tagh Fault during the Middle Miocene. *Can. J. Earth Sci.* 1–50 (ejes-2016-0090.R2).
- Zhao, H., Wei, Y.Y., Shen, Y., Xiao, A.C., Mao, L.G., Wang, L.Q., Guan, J.Y., Wu, L., 2016. Cenozoic tilting history of the south slope of the Altyn Tagh as revealed by seismic profiling: implications for the kinematics of the Altyn Tagh fault bounding the northern margin of the Tibetan Plateau. *Geosphere* 12 (3), 884–899.

- Zheng, H.B., Powell, M.A., An, Z.S., Zhou, J., Dong, G.R., 2000. Pliocene uplift of the northern Tibetan Plateau. *Geology* 28 (8), 715–718.
- Zhuang, G.S., Hourigan, J.K., Ritts, B.D., Kent-Corson, M.L., 2011a. Cenozoic multiple-phase tectonic evolution of the northern Tibetan Plateau: constraints from sedimentary records from Qaidam basin, Hexi Corridor, and Subei basin, northwest China. *Am. J. Sci.* 311, 116–152.
- Zhuang, G.S., Hourigan, J.K., Koch, P.L., Ritts, B.D., Kent-Corson, M.L., 2011b. Isotopic constraints on intensified aridity in Central Asia around 12 Ma. *Earth Planet. Sci. Lett.* 312 (1–2), 152–163.